BACHELOR THESIS

Analytical and Numerical Investigation of the Damping Behavior of a Quarter Wave Resonator using an Incompressible Approach

Autor:
Yujie Lian

Matrikel-No:
03699678

Betreuer:
Simon van Buren, M. Sc.
Prof. Wolfgang Polifke, Ph. D.

August 15, 2018

Technische Universität München
Fakultät für Maschinenwesen
Professur für Thermofluiddynamik
Prof. Wolfgang Polifke, Ph. D.

Erklärung

Hiermit versichere ich, die vorliegende Arbeit selbstständig verfasst zu haben. Ich habe keine anderen Quellen und Hilfsmittel als die angegebenen verwendet.

Ort, Datum	Yujie Lian

Acknowledgement

I would like to extend my sincere gratitude to my supervisor, Simon van Buren, for his instructive advice and useful suggestions for my thesis. I am deeply grateful for his help in the completion of this thesis.

Abstract

The work investigates the damping behavior of a Quarter wave resonator analytically and numerically, in which an incompressible approach is used. The Quarter wave resonator is investigated based on a methodology of decomposition that has been successfully used in the previous work of the Helmholtz resonator. The analytical investigation is implemented in MATLAB. The simulation in MATLAB contains two loops: an inner loop investigating the damping behavior in the frequency domain and an outer loop taking SPL into consideration. Iterations are applied in the outer loop to adjust the amplitude of velocity in order to make sure the SPL remains constant. The investigation is utilized to reveal the effects of the different proportion of the length of the resonator to the damping behavior. Besides, the dominance of the linear and nonlinear effect is also investigated. Furthermore, the numerical investigation is implemented in an open source software OpenFOAM. The mesh is generated by simplifying the resonator to a slice of it. Proper boundary conditions are chosen to maintain the accuracy of results and to achieve the perturbation of the incident excitation. The effect of different reference length and the mesh resolution is also investigated and the reference length and mesh resolution are set up properly. Then two approaches of obtaining the impedance of the neck are implemented in MATLAB and the results are compared. Afterward, the damping effect is evaluated. Overall, the results of the analytical investigation and numerical investigation are compared and the possible inaccuracy is pointed out.

Contents

Nomenclature

Roman Symbols

A_u	Amplitude of velocity	[m/s]
c_0	Speed of sound	[m/s]
C_d	Contraction factor	[-]
d_0	Diameter of the Quarter resonator	[m]
f, g	Riemann Invariants	[m/s]
l_0	Length of the backing cavity	[m]
l_0	Length of the neck	[m]
l_c	Length correction	[m]
l_e	Effective length	[m]
l_{ref}	Reference length	[m]
l_{sim}	Simulation length	[m]
l_{tot}	Total length of the Quarter resonator	[m]
p	Pressure	[Pa]
p_0	Atmospheric pressure	[Pa]
p_{ref}	Reference pressure	[Pa]
p_{rms}	Root square of pressure	[Pa]
P_r	Prandtl number	[-]
R	Refection coefficient	[-]
$R_{l,cor}$	Corrected real-valued constant	[-]

R_l	Real-valued constant	[-]
$R_{specific}$	Specific gas constant	[J/(kg K)]
s	Boundary layer parameter	[-]
T	Temperature	[K]
t	Time	[s]
T_0	Room Temperature	[K]
u	Velocity	[m/s]
Z	Impedance	[N s/m^3]
z	Normalized impedance	[-]
Z_o	Impedance of the neck	[N s/m^3]
Z_s	Specific impedance	[N s/m^3]
Z_{bc}	Impedance of the backing cavity	[N s/m^3]

Greek Symbols

γ	Ratio of specific heats	[-]
ρ	Density	[kg/m^3]
ρ_0	Ambient density	[kg/m^3]
σ	Porosity	[-]

Index and Superscripts

$\cdot'$	Fluctuating value
$\cdot_1$	Position 1 at the inlet of the neck of the resonator
$\cdot_2$	Position 2 at the outlet of the neck of the resonator
$\hat{\cdot}$	Fourier transform

Acronyms

CFD	Computational fluid dynamics	
FFT	Fast Fourier transform	
SPL	Sound pressure level	[dB]

1 Introduction

Combustion systems, such as the combustion chamber, are all facing fetal thermoacoustic instabilities, which may cause the failure of the whole system. These instabilities may occur due to feedback from unstable combustion processes and acoustical resonance within the system. When the fluctuating incident wave is reflected from the wall, it may in turns, affect the combustion process itself. When the amplitude of the wave is too larger, it may damage the whole system. In order to absorb sound, reduce sound reflection and increase the stability of the system, resonators are implemented in the combustion systems and also many other industrial systems. Thus, the resonator is a very essential device in many applications. There are basically two placement types of resonators, locally and non-locally reacting resonators. As for the non-locally reacting resonators, the openings of the resonators are placed so far that the incident angle of the acoustic wave affects the damping behavior of the resonator. As for the locally reacting resonators, the openings of the resonators are placed so close that the damping behavior of the resonator is irrelevant to the incident angle of the acoustic wave. This is also the most commonly used placement types of the resonator. So, in this thesis, the locally reacting resonators will be investigated. Further, three different types of the resonator are normally applied, Helmholtz resonator, half wave resonator and Quarter wave resonator. Among them, the Half-wave resonator has an open end and on the contrary, the Helmholtz resonator and Quarter wave resonator has a closed end. But since the open end is sometimes difficult to realize, the Helmholtz and Quarter wave resonator are more commonly used. The Helmholtz resonator is more popular in the applications and it has also been well investigated. Therefore, the Quarter wave resonator will be investigated in this thesis in order to fill the blank of the research to characterize the Quarter wave resonator. The name of the Quarter wave resonator is given because the length of the resonator is a quarter of the wavelength at the eigenfrequency. Comparing with the Helmholtz resonator, the Quarter wave resonator does not have a thin neck and a symmetrical backing cavity.

The goal of this thesis is to set up the analytical and numerical model of Quarter wave resonator and investigate its damping behavior respectively and contrastively. Both analytical and numerical investigation is based on the decomposition methodology proposed in [7]. The resonator will be decomposed into two parts: neck and backing cavity and they will be investigated separately. The damping behavior of the whole resonator will be investigated after adding the results of both parts together. Besides, the flow inside the neck should be considered as incompressible. This can be achieved when the length of the neck is short enough compared to the wavelength so that the neck can be considered as acoustically compact. If the neck is acoustically compact, the flow inside the neck can be considered as incompressible.

Moreover, the damping behavior of the resonator can be divided into two regions: the

linear region and the nonlinear region. The loss in the linear region is thermos-viscous loss mainly caused by the friction at the wall and the loss in the nonlinear region is mainly caused by the flow separation which is dominance at a higher velocity. This will be explained in Chapter 3.

In Chapter 4, the analytical investigation will be implemented in MATLAB based on the analogy of the resonator to a mechanical mass-spring-damper system. The damping behavior will be derived based on the governing equations and iteration will be done to make the SPL at the reference plane is the same as the target SPL. The effect of the different proportion of neck will be investigated in order to set the proper length of the neck. Then the dominance of linear and nonlinear will be investigated. The damping effect of the Quarter wave resonator at different SPL will be evaluated.

In Chapter 5, the numerical investigation is implemented in OpenFOAM. Since the incompressible approach is only applied in the neck, the simulation of the neck will be done numerically and the backing cavity will still be investigated analytically. The proper mesh will be generated and the proper mesh resolution will be selected based on the results of the simulation. Besides, the distance between the reference plane and the inlet of the resonator will be selected differently to check its independence to the simulation results, which also mentioned in [13]. At last, the results of the damping efficiency at different SPL will be evaluated.

In Chapter 6, the results from both analytical and numerical investigation will be compared and evaluated. The results show qualitative agreement. However, the deviations exist between the two investigations at the nonlinear damping effect. A correction coefficient will be implement applied to the linear part and the results after the correction will be evaluated.

2 Physical Background

This thesis investigates the damping behavior of the Quarter Wave Resonator using an incompressible approach. When an acoustic wave propagates in the resonator, losses will take place. Thus the reflected wave will be weakened. The damping behavior of the resonator indicates how the damping effect happens and how well can the resonator weaken the acoustical wave. In this section, several basic concepts related to this topic are introduced and assumptions, in order to simplify the case, are prescribed.

2.1 Wave Equations

In order to simplify the problem, it is necessary to simplify the acoustic wave propagation process and the media. Although these simplifications will bring certain limitations to the application of the results, these assumptions not only simplify the mathematical analysis but also make it possible to explain the basic rules and characteristics of sound wave propagation in a simple and straightforward way.

- The fluid should be perfect fluid, i.e., there should be no viscosity in the media and the wave should propagate without any loss.
- When there is no acoustic disturbance, the medium should be macro-static.
- When sound waves propagate, dense and sparse processes in the medium should be adiabatic.
- The acoustic wave should be with small amplitude, i.e. the pressure fluctuation should be much less than the mean pressure, the partial velocity should be much less than the speed of sound, the partial displacement should be much less than the wavelength and the incremental mass density should be much less than the static density.

Besides, this thesis investigates the resonator based on the one-dimensional simplification. In one-dimensional simplification, only one direction is taken into consideration. The one-dimensional continuity equation is basically the conservation of mass. It indicates that the difference between the mass of the inflow volume element per unit time in the medium and the mass of the outflow volume element should be equal to the increase or decrease in the mass of the volume element.

$$\frac{\partial \rho}{\partial t} + \frac{\partial (\rho u)}{\partial x} = 0 \tag{2.1}$$

In order to describe how the fluid reacts to the force acting on it, Newton's second law is applied to the particle system which helps to derive the momentum equation of the acoustic wave. It shows that the change of the total particle momentum in unit time is equal to the total force acting on the particles. This statement is often called the momentum-impulse principle.

$$\rho(\frac{\partial u}{\partial t} + u\frac{\partial u}{\partial x}) = -\frac{\partial p}{\partial x} \tag{2.2}$$

Both Eq.(2.1) and Eq.(2.2) are nonlinear, which means they are difficult to solve. Since the acoustical response is rather small compared to the ambient conditions, the notion is applied by dividing the state variables into two part: its value in the reference state and the perturbation that fluctuates around the reference state. In this thesis, the fluid can be assumed to be homogeneous, so that the conditions of the reference state, which consist of the ambient pressure p_0, ambient density ρ_0, ambient temperature T_0 and the mean acoustic wave velocity u_0, are in unity at all locations.

$$p = p_0 + p', \rho = \rho_0 + \rho', u = u_0 + u' \tag{2.3}$$

In order to simplify the Eq.(2.1) and Eq.(2.2), the variables in the those equations are replaced by the Eq.(2.3). Since the perturbations of the variables are sufficiently small, the product of perturbation can be neglected. Then the linearization of the equations can be achieved, i.e. the linearized *continuity equation* and the linearized *one-dimensional momentum equation.*

$$\frac{\partial \rho'}{\partial t} + \rho_0\frac{\partial u'}{\partial x} = 0 \tag{2.4}$$

$$\rho_0\frac{\partial u'}{\partial t} = -\frac{\partial p'}{\partial x} \tag{2.5}$$

Besides, with the similar linearization process, the *linear equation of state* can also be derived.

$$p' = c_0^2\rho' \tag{2.6}$$

Finally, by combining the Eq.(2.4), Eq.(2.5) and Eq.(2.6), the *one-dimensional wave equation* can be formulated:

$$\frac{\partial^2 p'}{\partial x^2} - \frac{1}{c_0^2}\frac{\partial^2 p'}{\partial t^2} = 0 \tag{2.7}$$

Noted that the speed of sound c_0 here can be treated as in the ideal gas. In this case, by applying the equation of speed of the ideal gas, the expression for the *speed of sound* of the ideal gas can be derived as:

$$c_0 = \sqrt{\gamma R_{specific} T_0} \tag{2.8}$$

where the γ stands for the *ratio of specific heats* and the $R_{specific}$ is the *specific gas constant.*

Since in many applications the sound wave can be considered as the plane wave which propagates in a 1-D manner, Eq.(2.7) can be decomposed into

$$(\frac{\partial p'}{\partial x} + \frac{1}{c_0}\frac{\partial p'}{\partial t})(\frac{\partial p'}{\partial x} - \frac{1}{c_0}\frac{\partial p'}{\partial t}) = 0. \tag{2.9}$$

According to Eq.(2.9), the solution of the wave equation can be obviously derived into two parts: incident and reflected wave. By using the Riemann invariants, it can be defined as

$$f = \frac{1}{2}(\frac{p'}{\rho_0 c_0} + u'), g = \frac{1}{2}(\frac{p'}{\rho_0 c_0} - u') \tag{2.10}$$

Conversely, the fluctuating velocity u' and the fluctuating pressure p' can also be derived by Eq.(2.10):

$$u' = f - g, p' = \rho_0 c_0 (f + g). \tag{2.11}$$

2.2 Acoustical Variables and Concepts

In this subsection, the variables and the concepts that are mentioned in the following work will be illustrated.

2.2.1 Impedance

Impedance acts as a very important property of the resonator in the frequency domain to describe its damping behavior. It shows how difficult it is to move the medium back and forth in the resonator. The impedance consists of two parts: a real part and an imaginary part. Among them, the real part is relevant to the Amplitude reduction and the imaginary part takes care of the phase shift. It can be derived by:

$$Z = \frac{\hat{p}}{\hat{u}}. \tag{2.12}$$

where the $\hat{\cdot}$ denotes the variables that are transformed from the time domain to the frequency domain by Fourier transform.

In order to make the impedance more straightforward to compare, the characteristic specific acoustic impedance is used to normalize the impedance. The characteristic specific acoustic impedance is calculated as follow:

$$Z_s = \rho_0 c_0. \tag{2.13}$$

Then the impedance is normalized by dividing Z_s in Eq.(2.13):

$$z = \frac{Z}{Z_S}. \tag{2.14}$$

2.2.2 Reflection Coefficient

Beside the impedance, another variable can be used to characterize the behavior of the resonator, the *reflection coefficient*, which shows to which degree the incident wave is reflected. The reflection coefficient is the ratio of the reflected g wave to the incident wave f:

$$R = \frac{\hat{g}}{\hat{f}}. \tag{2.15}$$

The reflection coefficient can also be calculated by the impedance:

$$R = \frac{Z - \rho_0 c_0}{Z + \rho_0 c_0} = \frac{z-1}{z+1}. \tag{2.16}$$

As the impedance is a complex number, the reflection coefficient will also contain a real part and an imaginary part. Thus, the gain of the reflection coefficient describes the reduction in amplitude and the phase shows the phase change of the waves due to the reflection effect.

2.2.3 Sound Pressure Level

Sound pressure level (SPL) refers to the size of the effective sound pressure relative to a reference value measured in logarithmic scale, and its relationship with the reference value is described in decibels (dB). The human hearing threshold (i.e. the lowest sound pressure for hearing) for a 1 kHz sound is 20 μPa, which is usually used as a reference value p_{ref} for the sound pressure level:

$$SPL = 20\log_{10}(\frac{p_{rms}}{p_{ref}})dB \tag{2.17}$$

Notice that the p_{rms} is the root mean square of the acoustic pressure. In this work, the reflection coefficient is investigated as a function of both frequency and the SPL. It is relevant to the dominance of the linear and nonlinear effect.

3 Principle of Methodology to the Investigation of Resonator

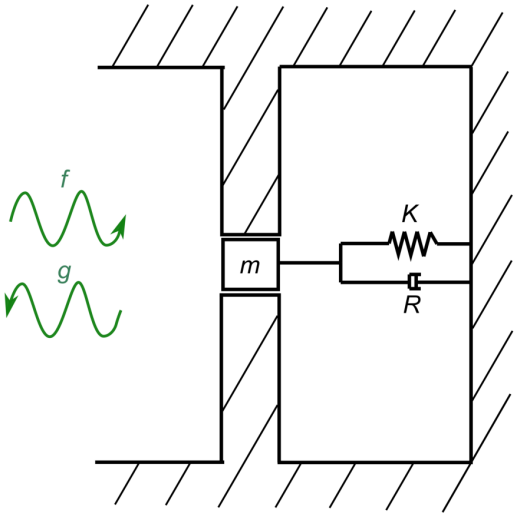

Figure 3.1: Analog of a resonator to a mechanical mass-spring-damper system.

The investigation of a resonator can analog to a mechanical mass-spring-damper system, see [4]. As shown in Figure 3.1, in which the flow in the neck is considered as a mass m and it oscillates inside the neck, the compressed and decompressed air in the backing cavity is considered as the spring stiffness K and the losses due to the friction and flow separation is represented by the damping coefficient R. In this case, the resonator can be regarded as a single degree of freedom oscillators. Therefore, the damping effect can be divided into two part:

- At the lower SPL, the damping effect is mainly caused by linear effect: the friction between the flow and the wall due to the viscosity. It takes place in the boundary layer of the flow
- At the higher SPL, the flow separation is triggered and vortices are generated, which lead to the dominance of the nonlinear effect. Most of the kinetic energy of the flow is dissipated by forming the vortices which cause the loss of the acoustic energy. The

higher the velocity is, the easier the flow separation occurs. When the velocity reaches a certain level, the nonlinear effect will dominate.

In order to investigate the resonator, Ingard and Ising[8] suggested the methodology which decomposes the resonator into two parts: the neck and the back cavity. This works resultful on the Helmholtz resonator and it is easy to separate the two parts in the geometry of the Helmholtz resonator. As shown in Figure 3.2, there is an obvious dividing line between the neck and the backing cavity. So the methodology of the decomposition is reasonable for a Helmholtz resonator. The investigation of this methodology has been done by Foerner [4] and the results of this methodology are validated by the experiment.

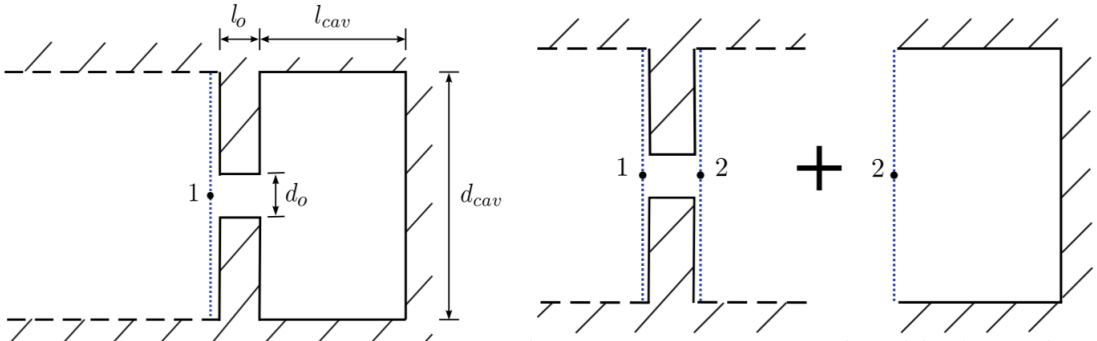

(a) Complete Helmholtz resonator

(b) Decomposition into neck and backing volume

Figure 3.2: Sketch of the considered geometry and reference cut planes 1and 2 for the decomposed Helmholtz resonator model from [13]

On the contrary, the geometry of the Quarter wave resonator does not have the obvious dividing line between the neck and the back cavity.

In this thesis, a similar methodology is applied also on the Quarter wave resonator. To implement this methodology, a specific length of the Quarter wave resonator is considered as the neck and the rest will be the backing cavity as shown in the Figure 3.3(b). In this way the impedance can also be decomposed into two parts: the impedance of the neck Z_o and the impedance of the back cavity Z_{bc}:

$$Z = \frac{\hat{p}'_1 - \hat{p}'_2}{\hat{u}'_1} + \frac{\hat{p}'_2}{\hat{u}'_1} \tag{3.1}$$

Since the length of the neck is short enough to be acoustically compact, the fluid inside can be considered incompressible. Obeying the conservation of the mass in the neck, the velocity u_1 at point 1 and the velocity u_2 at point 2 in the Helmholtz resonator are the same. Therefore, in Helmholtz resonator Eq.(3.1) can be transformed in to:

$$Z = \frac{\hat{p}'_1 - \hat{p}'_2}{\hat{u}'_1} + \frac{\hat{p}'_2}{\hat{u}'_2} = Z_o + Z_{bc} \tag{3.2}$$

Notice that due to the asymmetrical configuration in the Quarter wave resonator, the velocity u_1 at point 1 and the velocity u_2 at point 2 in the Quarter wave resonator are not the same. They have the relation as follow:

$$u_2' = \sigma u_1'. \tag{3.3}$$

In this case, Eq.(3.4) should be rewritten as:

$$Z = \frac{\hat{p_1'} - \hat{p_2'}}{\hat{u_1'}} + \sigma \frac{\hat{p_2'}}{\hat{u_2'}} = Z_o + Z_{bc} \tag{3.4}$$

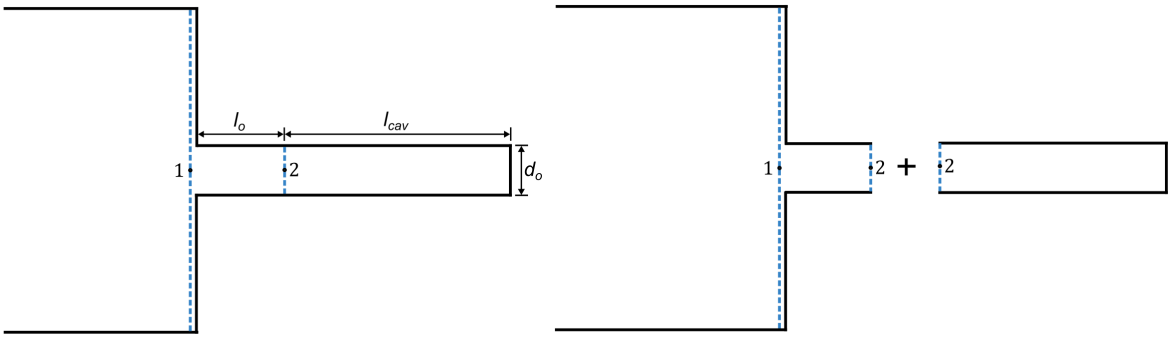

(a) Complete Quarter wave resonator

(b) Decomposition into neck and backing volume

Figure 3.3: Sketch of the considered geometry and reference cut planes 1and 2 for the decomposed Quarter wave resonator model

4 Analytical Investigation

The analytical part of the thesis will be carried out in MATLAB. It is still based on the decomposition of the resonator. Contrary to the Helmholtz resonator, the Quarter wave resonator has an area jump which leads to an asymmetrical configuration. In order to characterize the Quarter wave resonator with the similar methodology, a proper length of the neck should be chosen and the rest of the resonator should be considered as the backing cavity.

4.1 Test Case Geometry

The parameters of the Quarter wave resonator, which are investigated in this thesis, are not all selected from the previous cases. As shown in the name of this resonator, the total length of the Quarter wave resonator is a quarter of the wavelength at eigenfrequency. Since there is no actual experiment result for an actual Quarter wave resonator, the eigenfrequency of the Quarter wave resonator is set as 400 Hz and the total length is set up accordingly; Other parameters are set as in [3]:

	l_{tot} [mm]	d_0 [mm]	σ [%]
QW	214.5	6.35	1.56

Table 4.1: Parameters of the Quarter wave resonator .

where the l_{tot} is the total length of the Quarter wave resonator. As shown in the Figure 3.3, $l_{tot} = l_o + l_{cav}$

The length of the neck is not fixed in this part of the investigation and a length correction l_c, which accounts for the fluid that oscillates in front of the opening of the resonator, should also be taken into consideration. According to Ingard[7], l_c can be calculated as:

$$l_c = \frac{4}{3\pi} d_0. \tag{4.1}$$

Due to the asymmetry of the Quarter wave resonator, only the opening need the correction, which means the effective length $l_e = l_0 + l_c$.

Besides, the parameters of the resonator test environment is set as follow:

	T [K]	p_0 [Pa]	κ	R [J/(mol·K)]
QW	293.15	10^5	1.4	8.3145

Table 4.2: Parameters of environment .

where T is the room temperature, p_0 is the atmospheric pressure, κ is the heat capacity ratio of air and R is gas constant.

4.2 Governing Equations

As shown in the equation, the impedance of the orifice is closely related to the pressure drop between the position 1 and the position 2. According to Foerner [3, 4] and Cummings [1], the pressure drop of the Quarter wave resonator can be formulated as:

$$\Delta p' \approx \rho_0 \frac{1}{\sigma} l_e \frac{\partial u'}{\partial t} + R_l u' + \frac{1}{2}\rho_0 \frac{u'\left|u'\right|}{(C_d\sigma)^2} + \frac{1}{2}\rho_0 u'^2 (\frac{1}{\sigma^2} - 1) \tag{4.2}$$

On the right hand of this equation, the first term represents the pressure drop of inertia, which is without any loss. This term is derived by applying the incompressible Bernoulli equation to both ends of the neck. The second term is caused by the friction at the wall and R_l is a constant which used to characterize this thermo-viscous loss, see [11]. The third term is responsible for the flow separation assuming that all the kinetic energy of the vortex is dissipated and does not recover. C_d denotes the contraction factor, which is the ratio of the flow core area to the cross-section area of the resonator, see also [14]. At low SPL, $C_d = 1$ since there is no flow separation while at higher SPL, $C_d < 1$ since the flow separation takes place in the resonator. The sharper the edge of the resonator is, the easier it will be to form the flow separation and the stronger the flow separation will be, see [2] and [10]. The last term is the additional term comparing to the Helmholtz resonator due to the asymmetry geometry of the Quarter wave resonator, i.e., the area jump.

The R_l in Eq(4.2) is calculated in [11] as:

$$s = \frac{1 + \frac{\gamma - 1}{Pr^{\frac{1}{2}}}}{d_0} \cdot \sqrt{\frac{2\nu}{\omega}} \tag{4.3}$$

$$R_l = s\rho l_0 \omega. \tag{4.4}$$

where s denotes the boundary layer parameter, γ is the kinematic viscosity, Pr is the Prandtl number.

With Eq.(4.2), the impedance of the incompressible neck can be calculated by:

$$Z_o = \frac{\Delta \hat{p}'}{\hat{u}'} \tag{4.5}$$

Besides, according to decomposition, the impedance of the back cavity is calculated separately, see [12] and also Hersh[6]:

$$Z_{bc} = -i\sigma \cot(\frac{\omega l_{cav}}{c})\rho_0 c_0 \tag{4.6}$$

Notice that compared to the expression for the Helmholtz resonator, there is an additional open area ratio σ added in the equation due to the mass convention according to the Eq.(3.3) in the asymmetrical geometry of the Quarter wave resonator.

4.3 Analytical Setup

Since the reflection coefficient is a function of frequency and SPL, there are two steps to characterize the Quarter wave resonator analytically, see Figure 4.1. The first step, an inner loop is set up to investigate the Quarter wave resonator's damping behavior only in the frequency domain in which the SPL is not changed. Then the second step is an outer loop adding the SPL into consideration. The amplitude of the velocity fluctuation which relates to the actual SPL is adjusted by iteration until it converges. When the reflection coefficient is derived, the damping behavior of the Quarter wave resonator can be studied by analyzing the response of reflection coefficient and also the impedance accordingly to the changes of parameters.

After setting up the parameters, the fluctuation of the pressure and velocity should be set up first in order to derive the impedance and then the reflection coefficient. The flow is set as a velocity driven flow with a fluctuating velocity set as follow:

$$u' = A_u cos(\omega t). \tag{4.7}$$

Notice that the amplitude of the fluctuating velocity is not a constant value, it will be adjusted in the second loop to make the SPL constant on the reference plane.

The pressure of the resonator can be derived by the velocity in the time domain. According to Eq.(2.12), a Fourier transform is required to derive both velocity and pressure fluctuation in the frequency domain. It can be achieved by applying a function in MATLAB, Fast Fourier Transform. When doing the FFT to the pressure drop, there is derivative in the first term of the Eq.(4.2) needs to be dealing with. According to the properties of Fourier transform:

$$\frac{\partial \hat{u}'}{\partial t} = i\omega U'(\omega) \tag{4.8}$$

There are two ways to do the Fourier transform to pressure drop from the time domain to the frequency domain. One method is to do the derivative first and then do FFT, the other one is to directly use the properties of Fourier transform so that the derivative part can be spared. Both two methods have been tested and the result shows a very good agreement. In this part of the work, the first method is used.

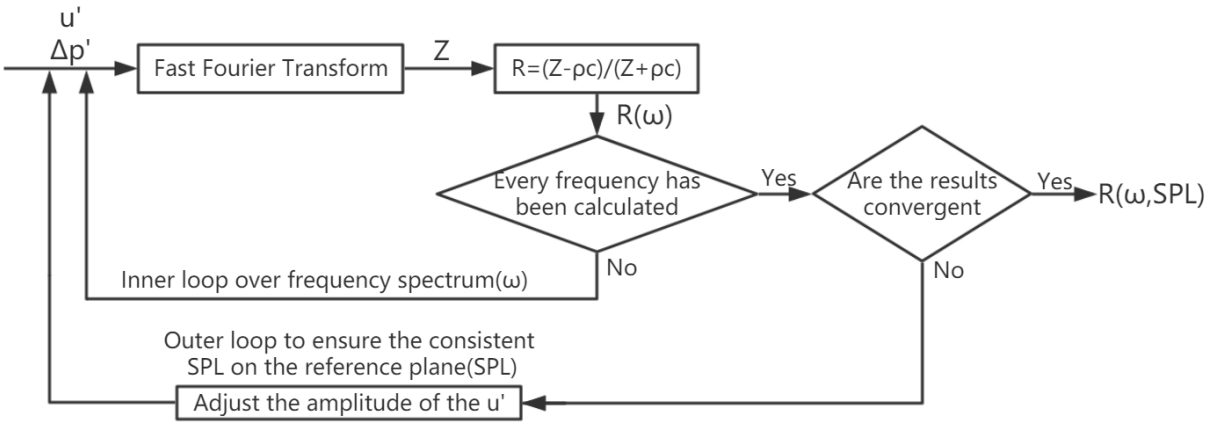

Figure 4.1: Workflow in MATLAB

4.3.1 Iteration process

After all this preparation, the damping behavior at a frequency range from 25 Hz to 700 Hz is investigated. However, the damping behavior of the resonator is also relevant to the SPL, so this is when the outer loop comes in. The goal of the outer loop is to make the SPL at the reference plane constant as the target SPL. The reason why it is needed is that the acoustic wave is damped significantly at the eigenfrequency. As the result of this, the actual SPL at reference plane will also reduce to a lower SPL. Whereas in this investigation, the damping behavior should be evaluated under a constant SPL.

To achieve that, the outer loop carries out iterations to adjust the amplitude of the incident wave's velocity, so that the actual SPL at every frequency could be consistent with the target SPL. To be more elaborate, in this stage, every amplitude of the velocity at every frequency in every loop will be modified, especially the amplitude around the eigenfrequency will be magnified. So that even though the damping behavior is most significant at the eigenfrequency, the actual SPL can remain consistent.

Notice that in the compressible simulation, it is the amplitude of the incoming wave f need to be adjusted, see[13] and the adjustment in incompressible is done by adjusting the amplitude of velocity:

$$A_u(\omega, SPL) = |1 - R(\omega, SPL)|\, 10^{SPL/20} \frac{\sqrt{2} p_{ref}}{\left|1 + R(\omega, SPL) exp(-i\omega 2 l_{ref}) \rho_0 c_0\right|}. \tag{4.9}$$

In the beginning, a constant velocity amplitude is assumed and then it is adjusted based on the reflection coefficient and the actual SPL. The velocity in each iteration oscillates until it converges to a stable value. When the difference between reflection coefficient in the last two iterations is smaller than the threshold value, e.g., 1e-6, the result from the last simulation is taken as the final result, which makes the SPL at the reference plane constant, see Figure 4.2. The gain of the reflection coefficient oscillates during the iteration process and it eventually converges to the approaching value. Notice that iterations needed at 120dB are much more than at the 70dB.

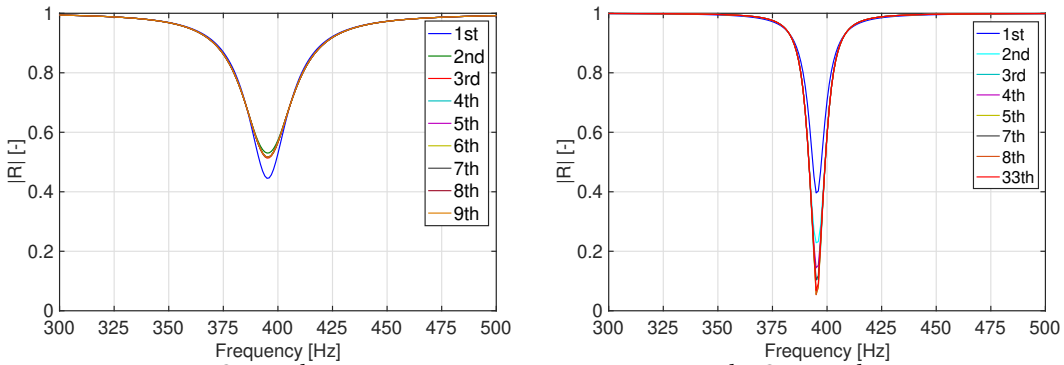

(a) SPL 70dB (b) SPL 120dB

Figure 4.2: The iteration process to derive the reflection coefficient at different SPL(70dB and 120dB)

The adjustment of the amplitude of velocity A_u is shown in Figure 4.3. The first guess of A_u is too low for the target SPL, so the second guess becomes much larger. But it is too large so that the third one is set to be a bit smaller. In this way, the amplitude of velocity finally approaches the approaching value. Also, notice that it only takes a few iterations at 70dB until the velocity amplitude approaches the final result; However it takes dozens of iterations at 120dB to eventually converge, which can be observed in Figure 4.3(b): the curve of velocity oscillates many times around the approaching value. These phenomena are caused by the dominance of the linear and nonlinear regime, which is explained in Section 4.4.2

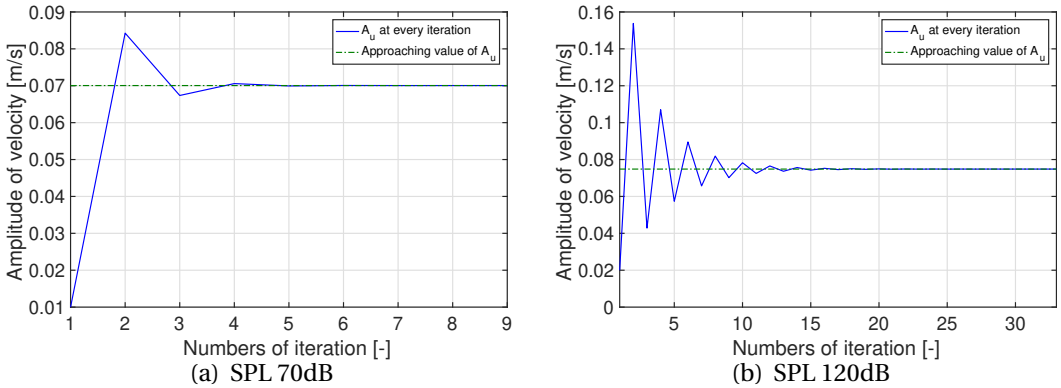

(a) SPL 70dB (b) SPL 120dB

Figure 4.3: The iteration of excitation amplitude at different SPL(70dB and 120dB)

The results of the iteration process are shown in Figure 4.4. Notice that u_{init} denotes the initial guess of the velocity and it is set the same at each frequency. However, the final velocity profile is completely different from the initial guess. The pattern is similar in both 70dB and 130dB. At the eigenfrequency, the velocity is much higher than the velocity at the frequency away from the eigenfrequency. The closer the frequency is to the eigenfrequency, the higher excitation is needed. At the frequency, which is far away from the eigenfrequency, the exci-

tation is significantly lower. This phenomenon matches with the theory well: At the eigenfrequency, the damping effect is extremely considerable; So that the excitation amplitude needs to be high enough to overcome the damping effect in order to maintain the constant SPL. On the contrary, the damping effect is much lower at the frequency away from the eigenfrequency. As the result, only low excitation is needed. Moreover, although the velocity profile is similar at both 70dB and 130 dB, the excitation amplitude at 130dB is much higher than that at 70dB. It is also reasonable according to the definition of SPL.

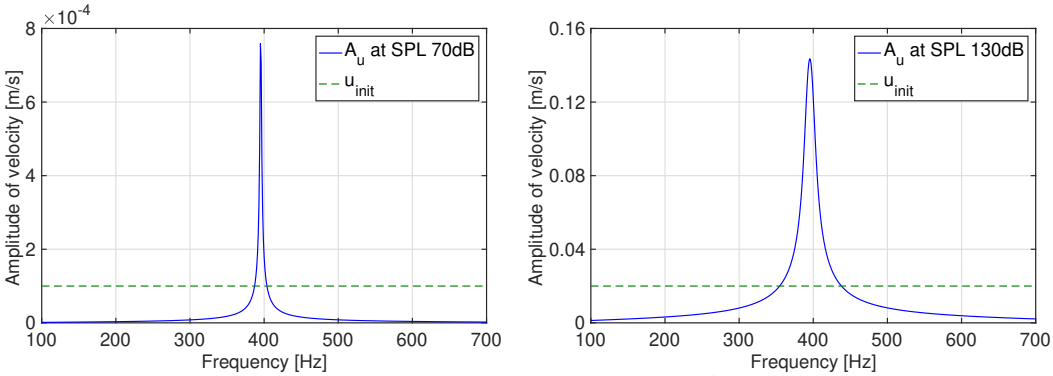

(a) SPL 70dB (b) SPL 130dB

Figure 4.4: Velocity profile at different SPL(70dB and 130dB)

4.4 Results of the Analytical Investigation

4.4.1 The Proportion of the Incompressible Neck

Because of the area jump in the Quarter wave resonator, it doesn't have a real neck; In order match, the method used in the investigation of the Helmholtz resonator, a suitable percentage of the Quarter wave resonator should be taken as the neck. As the result of different proportion, the damping behavior also differs from each other. The pattern of it can be used to determine the appropriate length of the neck in this analytical model when a corresponding experiment is implemented.

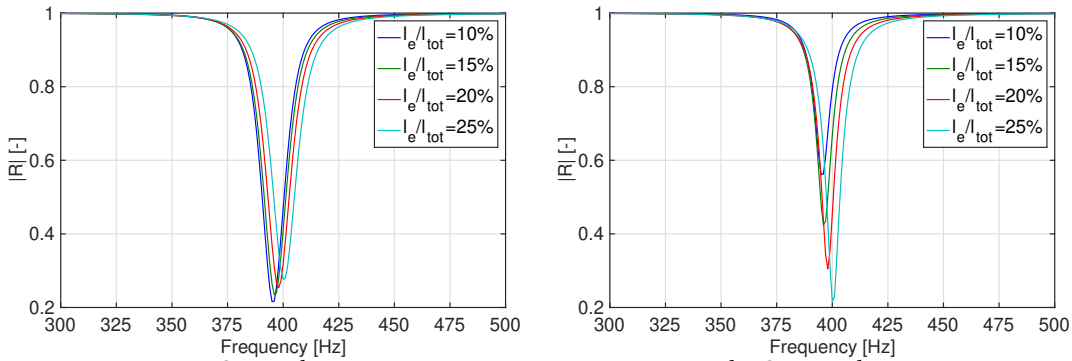

(a) SPL 70dB (b) SPL 130dB

Figure 4.5: Reflection coefficient at different proportion at SPL 70dB and 130dB

As shown in Figure 4.5, the results of reflection coefficient in SPL 70dB and 130dB are extremely different. As for the result at the lower SPL 70dB, the eigenfrequency differs at the different proportion of the neck. The larger the proportion, the higher the eigenfrequency; When the proportion is set to be 25%, the eigenfrequency matches perfectly at the target frequency and the length of the neck equals to 6.25% of the wavelength, which can still be considered as acoustically compact. Along with the increase in proportion, the gain of the reflection coefficient also increases slightly. On the contrary, the trend of the changes goes into the completely different direction at the higher SPL 130dB. The only similar result at 130dB is that the eigenfrequency also moves to a higher frequency when the proportion of neck increases. Notice that the gain of the reflection coefficient at eigenfrequency decreases dramatically from 0.6 to 0.2. These results show that the damping behavior at higher SPL has a stronger dependence on the proportion of neck than that at the lower SPL. This phenomenon can be explained by the investigation of impedance.

Besides the reflection coefficient, the impedance is also a very essential value to characterize the damping behavior of the resonator. On the one hand at the lower SPL, according to Figure 4.6, the resistance rises almost the same amount over the whole frequency spectrum at the different proportion of the neck. The increase of the resistance is linear to the increase of the proportion. This is reasonable because, at lower SPL, the damping behavior remains in the linear regime. The excitation of the acoustic incident wave is not intensive enough to

trigger the flow separation and the dissipation is mainly caused by the friction between the fluid and the wall. Since the energy loss due to the friction has a linear relation to the length of the wall, i.e., in this case, the length of the neck. The increase of resistance is also in a linear manner. As for the reactance, the deviation is quite small compared to the resistance. There is a slight deviation at the lower frequency but at the higher frequency, the resistance remains the same. The deviation between different cases decreases with the increase of the frequency. However, this deviation can be neglected compared to the resistance.

On the other hand at the higher SPL, the resistance is no longer in the linear regime see Figure 4.7. In this case, the nonlinear effect plays the dominant role. When the proportion of the neck increases, the whole resistance also increase. Moreover, the eigenfrequency at different proportion also changes. It also moves to a higher frequency which is similar in the lower SPL case. As for the reactance, the situation at higher SPL is identical with that at lower SPL. With this pattern, the more reasonable proportion can be set according to the experiment.

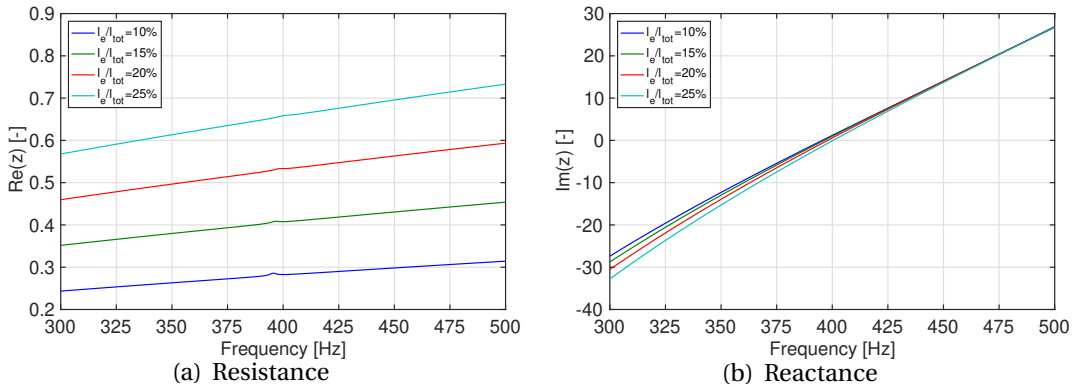

(a) Resistance (b) Reactance

Figure 4.6: Impedance at different proportion at SPL 70dB

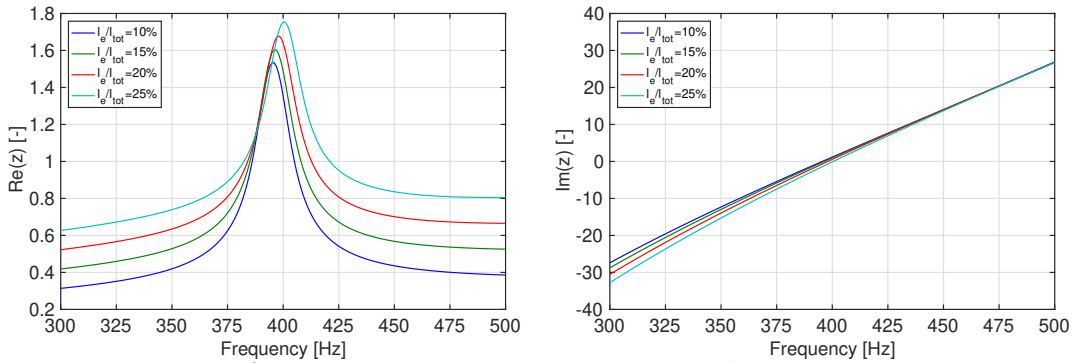

(a) Resistance (b) Reactance

Figure 4.7: Impedance at different proportion at SPL 130dB

4.4.2 Dominance of Linear and Nonlinear Effect

A resonator behaves in the linear regime only when the partial velocity is extremely small, which only occurs when the SPL is accordingly small. Because SPL is a value that shows the strength and the intensity of an acoustic wave and it is defined by the RMS of the amplitude of the pressure according to Eq.(2.17). In this case, the damping behavior of the resonator would be intensively depending on the frequency while on the contrary, the SPL plays only a less important role. When the SPL is relatively high, the flow separation will be triggered, which mainly responsible for the nonlinear effect.

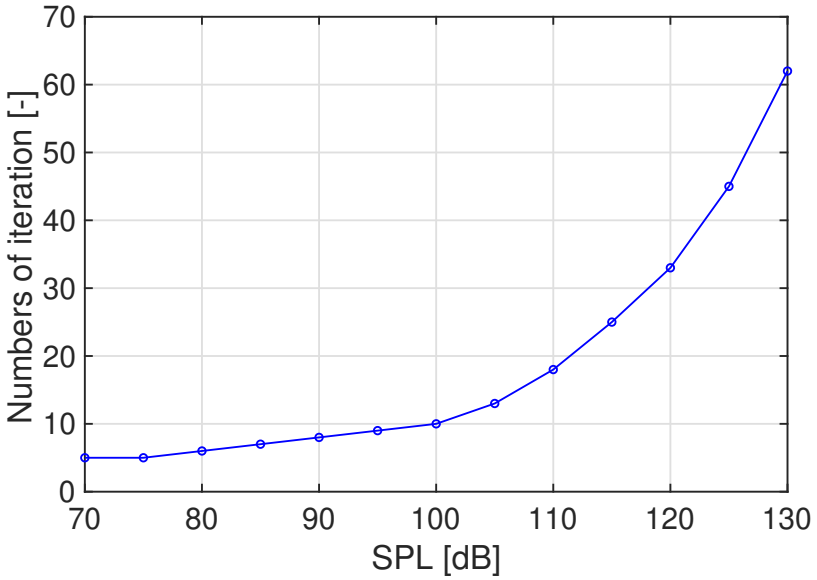

Figure 4.8: Numbers of iteration at different SPL

In order to study the dominance of the linear and nonlinear effect, several aspects can be taken into consideration. Firstly, times of iteration, which is needed to converge to the approaching value, can show the dominance in different SPL. When the SPL is low, the linear effect takes the dominant part of the resonator's behaving manner. As a result of this, the reflection coefficient can be seen as a pure function of frequency. The iteration needed to derive the actual reflection coefficient might only need a few times to reach the final result. Conversely, the situation at the higher SPL is very different. When the SPL is set to be high enough, the nonlinear effect, i.e., the flow separation dominates. In this case, the reflection coefficient is also dependent on the SPL. Hence, the iteration takes much more times to converge at the final result, because the starting value of the amplitude of the velocity leads to a considerable deviation from the actual SPL to the target SPL, which needs a lot more iterations to converge, see Figure 4.8. At the lower SPL it only takes around 5 iterations for the gain of reflection to converge, but at the higher SPL, it takes almost 65 iterations. The times of iteration increase slightly at the lower SPL, but it increases much more rapidly at the higher SPL. These results indicate that the nonlinear effect takes an increasingly dominant part with

an increasing SPL.

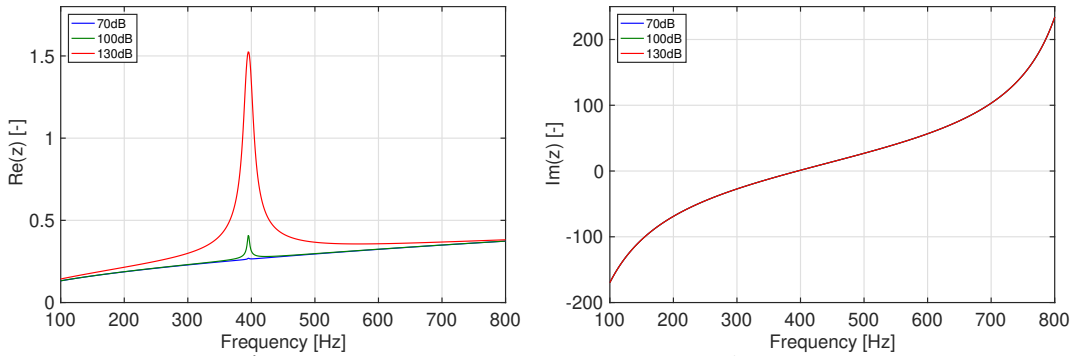

(a) Resistance (b) Reactance

Figure 4.9: Normalized impedance of the neck at different SPL(70dB and 130dB)

Secondly, the evidence of the dominance of both effect can also be found in the impedance. As shown in Figure 4.9, when the SPL is 70dB, the resistance stays in the linear regime and the nonlinear effect barely influences the impedance. The resistance increases linearly along with the increase of frequency. Compared to 70dB, the resistance at 100dB has a considerate deviation from the linear regime at the eigenfrequency, which indicates that the flow separation is triggered and the nonlinear effect starts to exceed the linear effect. Notice that at 100dB, the nonlinear effect has not taken the dominant part yet, since the excitation is not strong enough and energy loss due to the flow separation is not large enough. However, the resistance at 130dB shows a completely different manner. The resistance at eigenfrequency rises dramatically to almost 6 times larger than the resistance in the linear regime. This result suggests that the nonlinear effect becomes the dominance at 130dB. Moreover, this significant deviation takes place only at the frequency near the eigenfrequency; But the resistance is in good agreement at both ends of the frequency spectrum away from the eigenfrequency. This indicates that the nonlinear effect can only happen at eigenfrequency. The nonlinear effect cannot be triggered at the frequency away from the eigenfrequency even at the higher SPL. As for the reactance, the results from both SPLs remain the same which suggests that the reactance of the neck is irrelevant to the excitation amplitude. These results validate to the results and conclusion in [9] and also Eq.(4.2).

4.4.3 Damping Behavior at Different SPL

The damping behavior of a resonator is not only related to the frequency but also the SPL. In this part of the thesis, it is investigated more explicitly in term of SPL. Before analyzing the results, one more concept needs to be explained. At the eigenfrequency, the reactance of the resonator is zero, which only leaves the resistance to affect the gain of the reflection coefficient. According to Eq.(2.16), the optimal normalized resistance should be equal to one. In this case, there should be no reflection at all. Therefore the closer the normalized resistance to one, the closer the reflection coefficient to zero, i.e., the better damping behavior the resonator has. When the normalized resistance at eigenfrequency is below the optimal value one, the resonator is categorized as normal-damped. When the normalized resistance at eigenfrequency is larger than the optimal value one, the resonator is called over-damped. The main effect of these to the damping behavior is that, if the resonator is normal-damped, the gain of the reflection coefficient decreases with the increasing SPL; On the contrary, if the resonator is over-damped, the gain of the reflection coefficient also increases with the increasing SPL. This is also mentioned in [3].

As shown in Figure 4.10, the normalized resistance increases from 0.3 at 70dB to 1.5 at 130dB. The increasing rate of the resistance is rather small at the lower SPL, but it rises along with the increase of the SPL. As the result, the resistance grows more rapidly at the higher SPL. Notice that the normalized resistance exceeds 1 at around 120dB and the damping behavior of the resonator changes from normal-damped to over-damped.

It is more clearly shown in Figure 4.11 how the normal-damped and over-damped behaves. The gain of the reflection coefficient decreases until 120dB and it starts to increase after it exceeds 120dB. Even though the simulation is only done at the SPL up to 130dB, it is still conjecturable that the gain of the reflection coefficient will keep on increasing afterward.

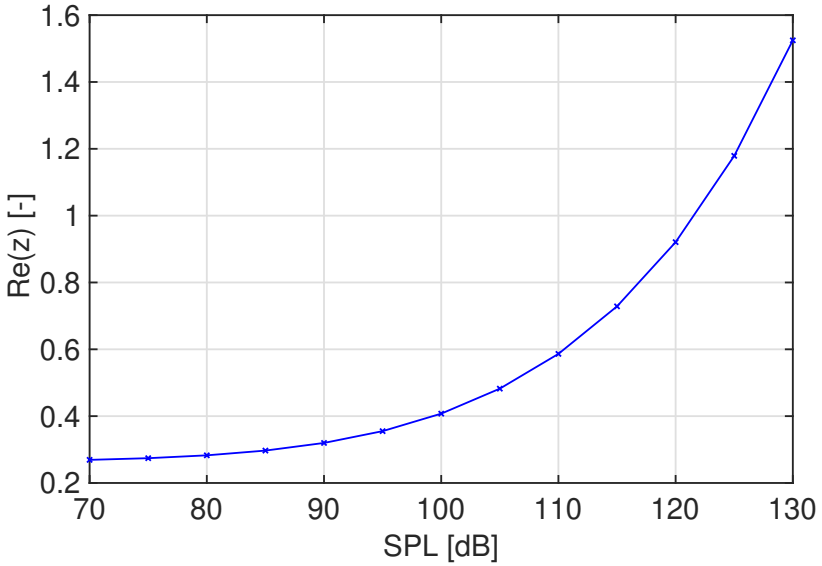

Figure 4.10: Normalized resistance of Quarter wave resonator at different SPL

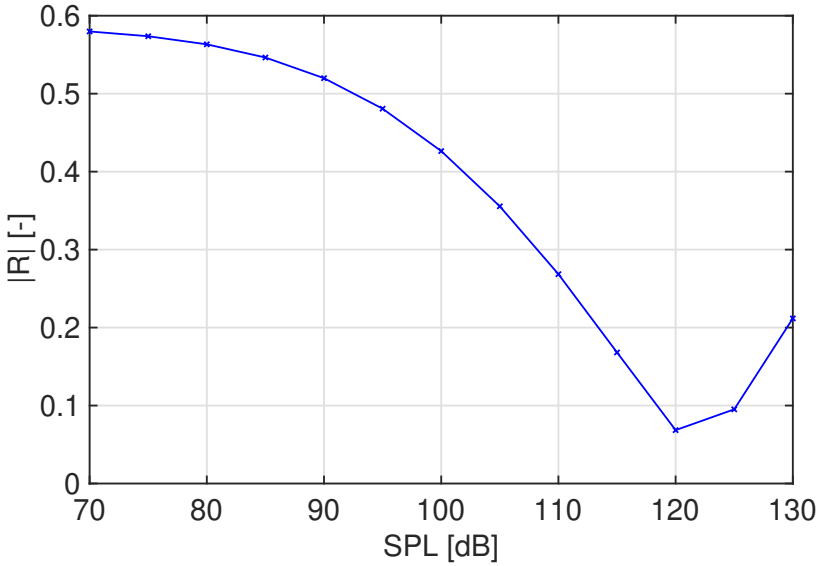

Figure 4.11: Gain of reflection coefficient of Quarter wave resonator at different SPL

5 Numerical Investigation

The numerical investigation is implemented on OpenFOAM. The version of this thesis using is 2.3.x and the working environment is Ubuntu 14.04. Moreover, the PIMPLE solver is used due to the incompressible assumption. Notice that the numerical simulation is not used for the entire resonator but only the neck, for the incompressible approach is only applied on the neck, not the backing cavity. The backing cavity will still use the analytical method as explained in chapter 2. For the workload of the numerical simulation takes up too much time doing simulation at the whole frequency spectrum, the numerical investigation will only be done at the eigenfrequency.

5.1 Test Case Geometry

Since the incompressible approach is only utilized on the neck of the resonator, the case geometry of the numerical simulation only contains a small space in front of the resonator and the incompressible neck as shown in Figure 5.1. The geometry parameters of the resonator will be the same as the previous analytical model so that the results of both models can be comparable.

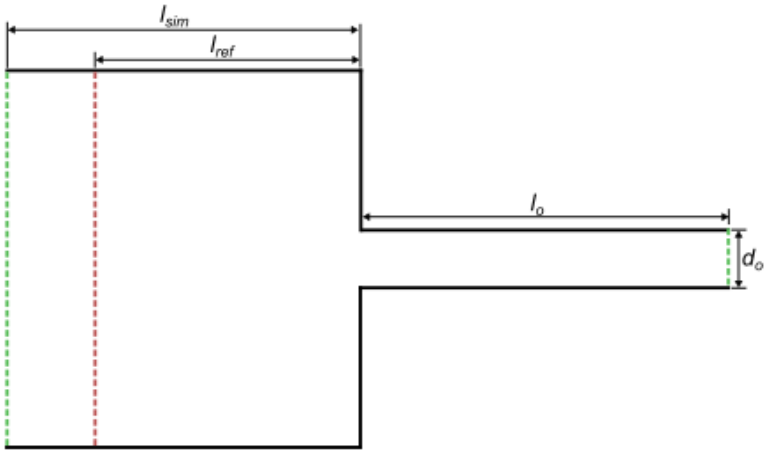

Figure 5.1: Test Case Geometry

In order to set up the proper case geometry, several simulations have been implemented. As shown in Table 5.1, the reference length has been set to be different, in order to investigate

	l_{ref} [mm]	$Re(z_o)$ [-]	$\Delta Re(z_o)$ [%]	$Im(z_o)$ [-]	$\Delta Im(z_o)$ [%]
Case 1	25	0.3743	-	9.0249	-
Case 2	35	0.3746	0.08	9.0135	0.13

Table 5.1: Results of cases with different reference length

its effect. The simulation results show only a slight deviation in the impedance, which can be neglected. According to [13], the simulation result should be independent of the position of the chosen reference plane. These simulation results validate the conclusion in [13].

Furthermore, the proper simulation domain is also investigated in this work. As the boundary conditions of this incompressible simulation are defined through prescribed oscillated velocity and fixed pressure value, the vortices should not across the simulation domain, because this is not accounted for the boundary treatment. In [13], the simulation domain is extended on both sides of the Helmholtz resonator in order to avoid the vortices crossing the simulation domain. However, in this work for the Quarter wave resonator, the simulation domain is only extended before the inlet, since in the Quarter wave resonator, the backing cavity is the same size as the neck. The vortices dissipate faster in the thin backing cavity, so there is no need to extend to the simulation domain on the outlet side. The simulation in this work is set up be far enough so that the vortices will not reach the border of the simulation domain.

5.2 Meshes

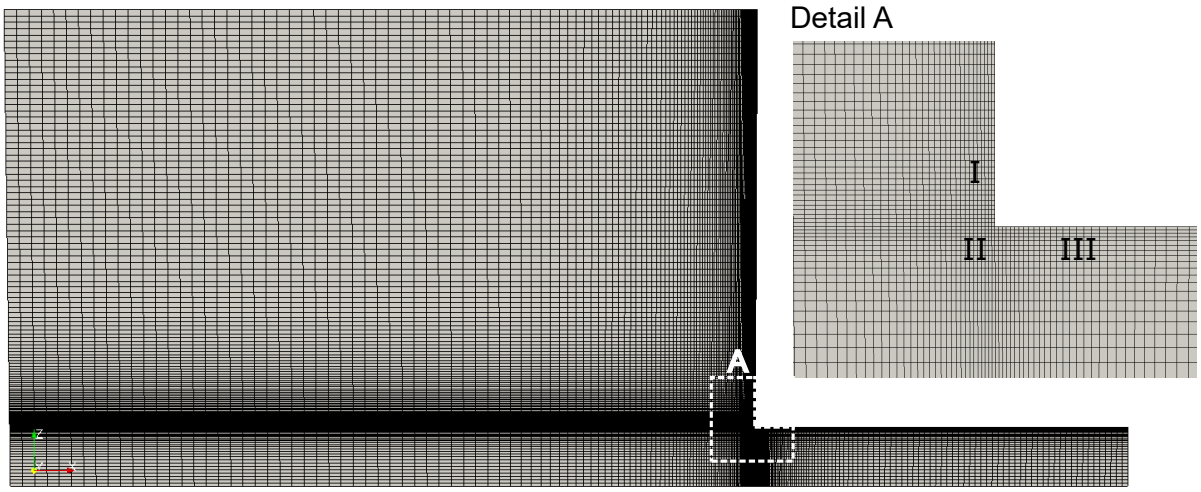

Figure 5.2: Mesh

Notice that the σ is the porosity of the resonator. It can be calculated as the ratio of the cross-sectional area of the duct and neck; Based on the mass conservation, it can also be derived the relation of the velocity.

There are two important setups of the meshes which should be taken care of. Firstly, the meshes near the no-slip wall, see section III in Figure 5.2 , should have a relatively higher resolution so that the friction within the boundary layer can be well captured. The friction is a very essential component of the resonator character which contributes a lot to the resistance of the impedance. So the resolution should be high enough so that the velocity gradient can be revealed. Simulations with higher and lower resolution have all been implemented, the results show that the simulation with higher resolution near the wall has slightly higher resistance. The deviation between the case with different resolution is relatively small. As explained before, the friction is one of the major cause of the resistance, so this result is consistent with the theory. Besides, the cell resolution in the section I should also be high enough. Even though the friction at that section has an only minor effect on the resonator, it is still necessary not to neglect it. Secondly, the cells around the corner, which is the section II in Figure 5.2, should also have higher resolution and shape should be close to the square. Due to the area jump, the velocity changes rapidly at the corner and vortex is triggered. Thus a well-refined mesh is required to capture the velocity gradient smoothly and explicitly.

Several simulations are done to investigate the dependency of the result to the mesh resolution. As shown in the Table 5.2, case 1 is for the lower resolution and case 2 is for the higher resolution. Even though the number of cells in case 2 is almost 170% to that in case 2, the deviation of both resistance and reactance in no more than 2.5%. This indicates that the mesh is fine enough to capture the damping effect so that even though there is a huge difference in the number of cells, the deviation of results is small enough to be neglected. But in order to

ensure the simulation is more accurate, all the simulations are done in higher resolution.

Moreover, higher grading in the normal direction to the wall can achieve the high resolution, but it also leads to the cells far away from the wall have a rather higher length-width ratio. This may lead to a problem, but in this simulation, no fetal problem has been found.

	number of cells [-]	$Re(z_o)$ [-]	$\Delta Re(z_o)$ [%]	$Im(z_o)$ [-]	$\Delta Im(z_o)$ [%]
Case 1(not refined)	21131	0.3663	-	9.1629	-
Case 2(refined)	34800	0.3743	2.18	9.0249	1.51

Table 5.2: Results of cases with different cell resolution

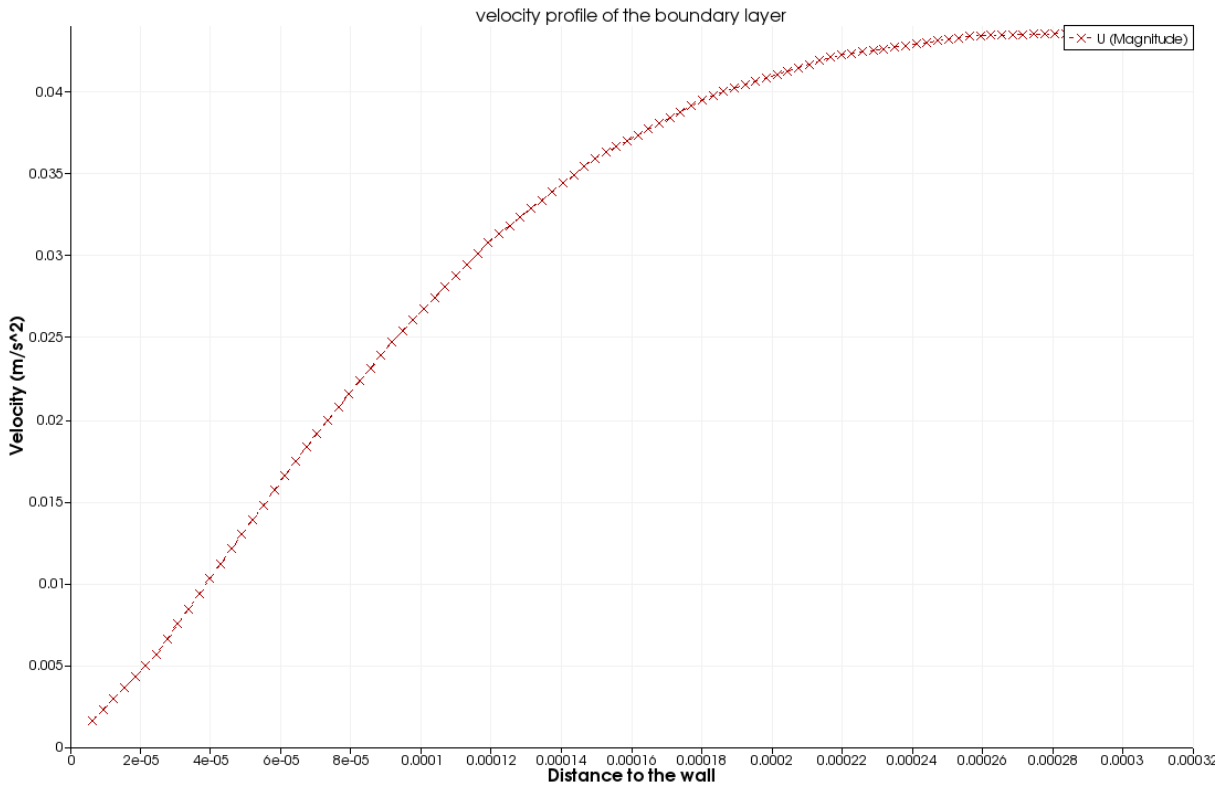

Figure 5.3: Velocity profile of the boundary layer

5.3 Numerical Setups

OpenFOAM[5] is a framework for developing application executables that use packaged functionality contained within a collection of approximately 100 C+ libraries. OpenFOAM is shipped with approximately 250 pre-built applications that fall into two categories: solvers, that are each designed to solve a specific problem in fluid (or continuum) mechanics; and utilities, that are designed to perform tasks that involve data manipulation. The solvers in OpenFOAM cover a wide range of problems in fluid dynamics. The solver used in this numerical investigation is PimpleFOAM. It is a large time-step transient solver for incompressible, turbulent flow[5], but instead of turbulent flow, laminar flow will be investigated.

5.3.1 Boundary Conditions

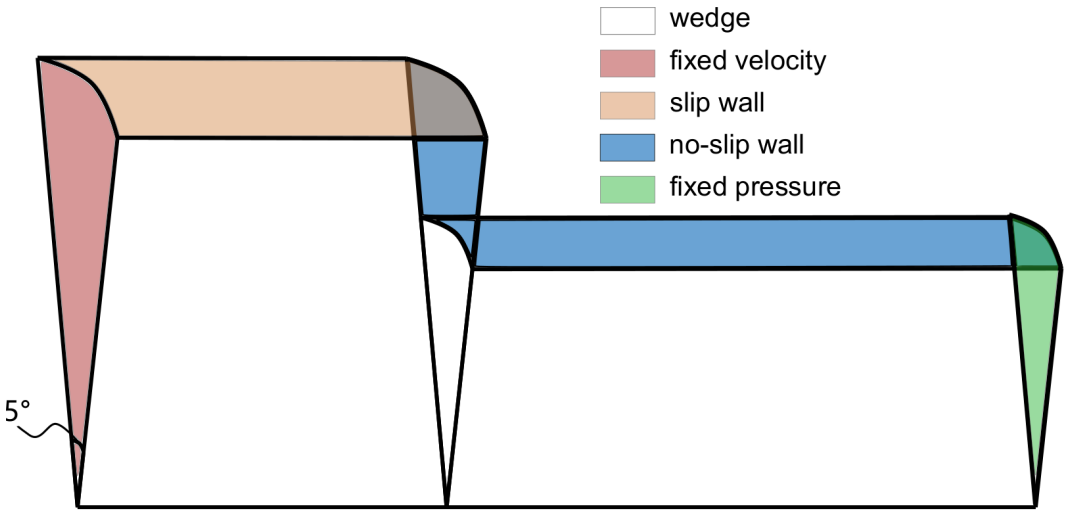

Figure 5.4: Boundary conditions of the case

Since the geometry of the resonator is centrosymmetric, the numerical investigation can be simplified to a small slice of the resonator, see Figure 5.4. This can be achieved in the OpenFOAM by simply using the *wedge* boundary condition on the symmetry plane. The result of this simplification should be the same as the full geometry but saves much time and effort. Notice that in this model, only one resonator is investigated, so the porosity is presented by the ratio of the circular sector of the two cross-section area.

The boundary condition is one of the most important setups in numerical simulations. The boundary conditions in this work are set mainly based on [13]. One of the key to set up the boundary conditions in this work is to set up the boundary condition of the inlet and the outlet correctly. The boundary condition of the inlet is defined as velocity-driven and the velocity is oscillating as the excitation to the resonator. In order to achieve this, the boundary condition *groovy bc* is utilized. This boundary condition is basically a mixed-BC where value, gradient and valueFraction are specified as expressions instead as fields. As for the outlet,

the boundary condition is defined as fixed pressure to meet the mass convention, since the incompressible approach is utilized in this work. The wall of the duct is set as the slip-wall. This boundary condition indicates that no boundary layer is developed near the wall and thus no friction has taken place. In this case, the velocity can maintain constant, see the same setup in [13]. As for the wall in the neck, it is defined as a no-slip wall, since the friction in the neck is one of the most essential components in the damping effect of the resonator. Moreover, the wall outside the neck is also set as no-slip. Even though the friction there is much smaller than the friction in the neck, it is still necessary for an accurate investigation of the resonator.

Since the numerical simulation is done only in the incompressible neck, in order to investigate the damping behavior of the whole resonator, the backing cavity is investigated analytically basing on the Eq.(4.6) and then the two results will be combined.

5.3.2 Evaluation Approaches

In the numerical part, there are two approaches to derive the impedance of the neck see[13]. The workflow of the two approaches is shown in Figure 5.5

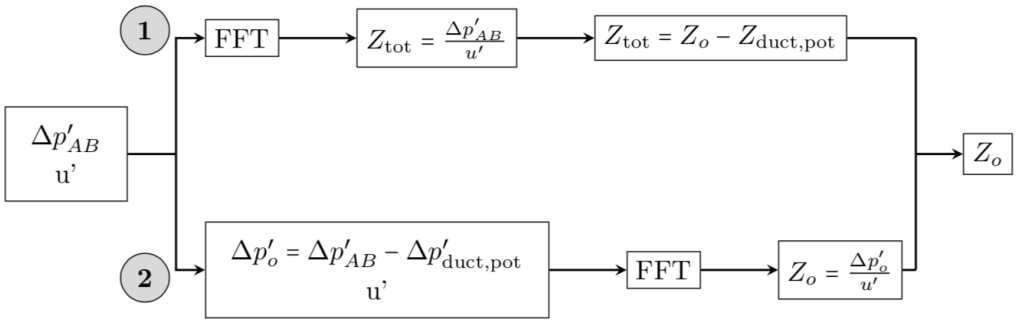

Figure 5.5: Workflow of two approaches to derive the impedance of the incompressible neck from [13]

According to [13], in approach 1, the total impedance is calculated first, then impedance from the reference plane to the inlet of the resonator, which is denoted as $Z_{duct,pot}$, is subtracted to get the impedance of the neck. The $Z_{duct,pot}$ for the Quarter wave resonator can be calculated by:

$$Z_{duct,pot} = i\rho\omega l_{ref} u'. \tag{5.1}$$

where l_{ref} is the distance between the reference plane to the inlet of the resonator, see Figure 5.1.

On the contrary in approach 2, the pressure drop between the reference plane to the inlet of the resonator, which is denoted as ΔP_{duct}, is subtracted first, then the neck impedance is derived directly. The ΔP_{duct} for the Quarter wave resonator can be derived by:

$$\Delta P_{duct} = \rho l_{ref} \frac{\partial u'}{\partial t}. \tag{5.2}$$

where $\frac{\partial u'}{\partial t}$ can be derived using MATLAB function $diff$.

The results should be the same due to the mathematically Fourier transform properties. It is confirmed in the [13] that the results from both approaches are in good agreement. There was only a considerably small deviation between the two approaches. In this work, both approached are all being tested at lower SPL in the Frequency spectrum near the eigenfrequency.

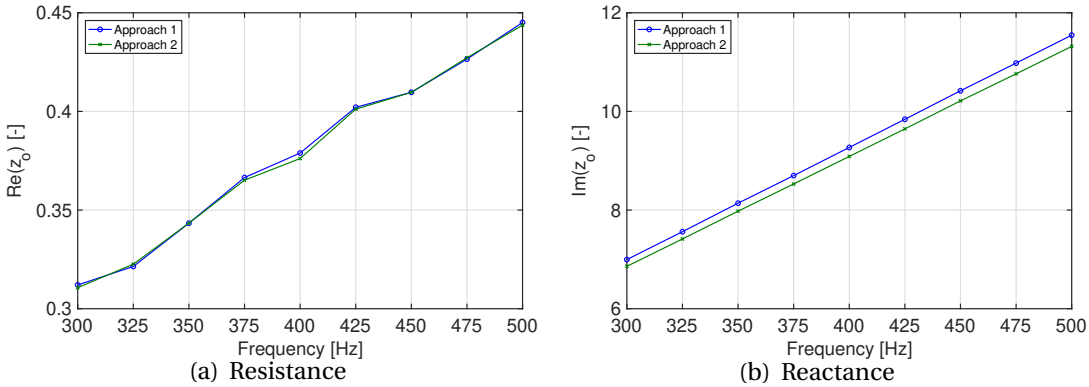

(a) Resistance (b) Reactance

Figure 5.6: Normalized resistance and reactance of the impedance of the neck obtained from different evaluation approaches

As shown in Figure 5.6, normalized resistance and reactance show good agreement. The resistance is extremely similar and the deviation between the two approaches is also small. More deviation has taken place in the reactance. Even though the shape of the reactance plot is the same, the reactance obtained from approach 1 is constantly slightly larger than that obtained from approach 2. However, these discrepancies can be acceptable and it is validated in [13]. In this part of the investigation, the approach 2 is utilized.

5.3.3 Iteration Process

The iteration process is also necessary for the numerical simulation. However, this can not be done in the OpenFOAM and part of it has to be done in MATLAB. The process is described as follow: firstly, the data is withdrawn from OpenFOAM and then is inputted into MATLAB. In MATLAB the impedance and the reflection coefficient are calculated analytically. Based on Eq(4.9), an adjusted velocity amplitude is derived. Afterward, the new velocity amplitude is implemented in the OpenFOAM and a new simulation starts. This iteration process stops when the amplitude of velocity or the reflection coefficient converge to approaching value. As shown in Figure 5.7, the amplitude of velocity oscillates around the approaching value. The more times the iteration has, the closer it is to the final result. Notice that the iteration process at the higher SPL level needs more times of iteration. It takes a dozen times at, for example, 120dB. On the contrary, the iteration processes at lower SPL, SPL below 100dB in this work, need only one simulation as long as the initial guess of amplitude is not too far from the final result. The reason for this has been already explained in the previous chapter. The accuracy of the iteration in OpenFOAM is not as good as that in the analytical investigation since OpenFOAM is much more comprehensive than MATLAB. It needs much more iterations to reach the accuracy in MATLAB and it is not necessary since the accuracy now is enough for the current investigation.

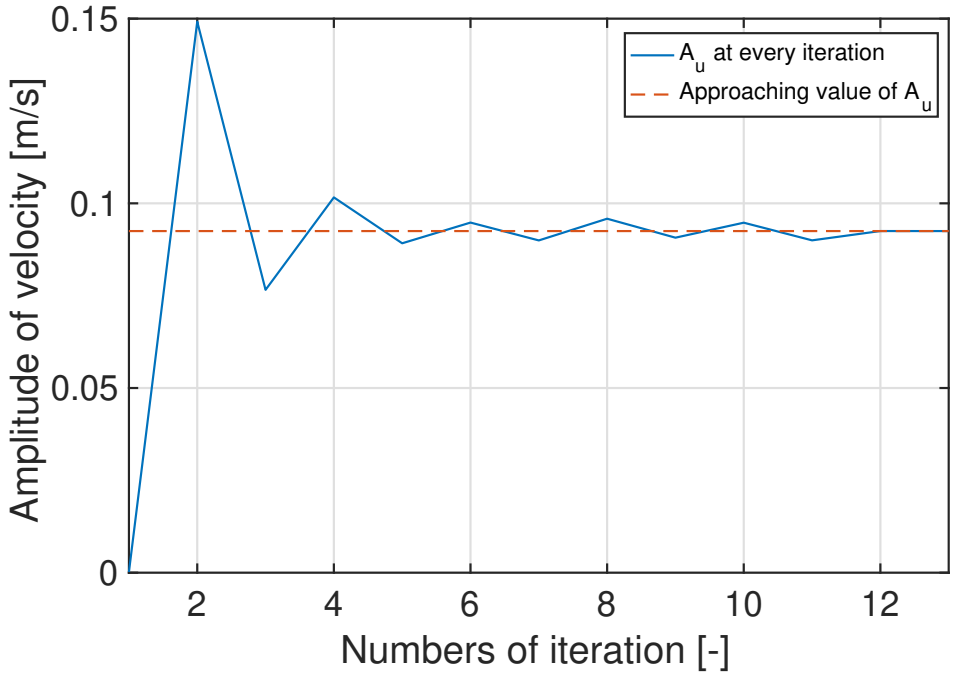

Figure 5.7: The iteration of excitation amplitude at SPL 120dB

The focusing point of this thesis is the damping behavior at the eigenfrequency. However, in order to make sure the method used in the analytical model also works in the numerical

model. Thus, several simulations are done in the lower SPL at 70dB. As shown in Figure 5.8, the velocity profile shows the same pattern as that in the analytical investigation. even though the initial guess of the velocity is the same at every frequency, it ends up at a different value. The velocity amplitude at both ends of the frequency spectrum is rather low, while it increases rapidly to the maximum at the eigenfrequency. The curve of the velocity profile is discontinuous and not smooth since only limited simulations have been done in the frequency domain.

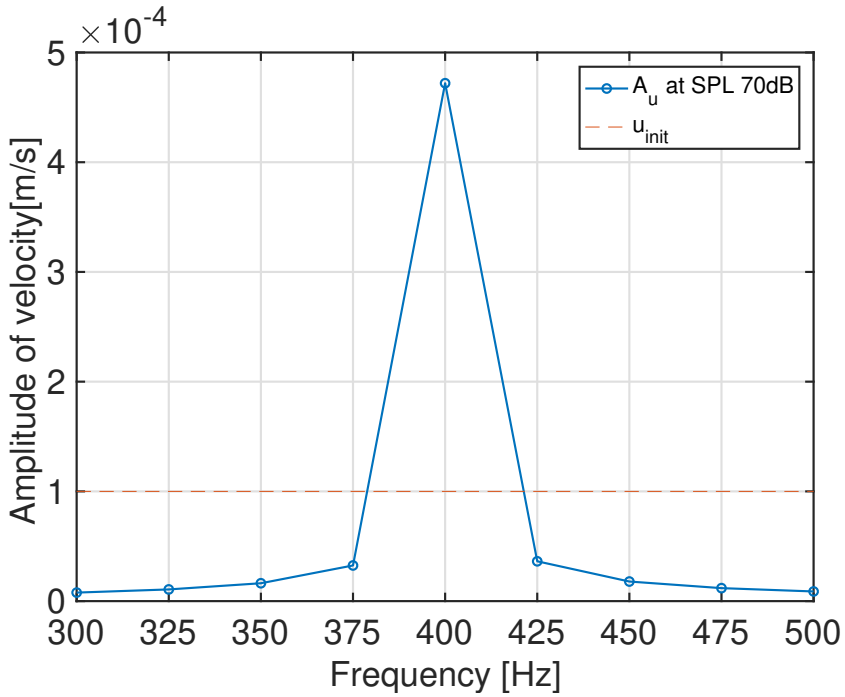

Figure 5.8: Velocity profile at SPL 70dB

5.4 Results of the Numerical Simulations

5.4.1 Original Data from OpenFOAM

In the actual simulation process, the data of every time step at every cell has been computed. However, these data cannot reveal the damping behavior without post-processing. In this work, the velocity and the pressure at the reference plane are calculated as the average value of data on the whole reference plane. As shown in Figure 5.9, velocity and the pressure are harmonic. Since the flow in this numerical simulation is set to be velocity-driven, the pressure is the response of the excitation. Notice that there are changes taken place in amplitude and phase. The amplitude of the pressure changes obviously and its phase also shifts a little bit backward. The change in amplitude will contribute to the resistance of the impedance and the shift in phase will lead to the reactance. Moreover, in the numerical simulation, the time has been set to be exactly 10 periods in order to let the acoustic wave fully propagated in the resonator and only the last period is inputted to the analytical computation in MATLAB.

Moreover, the velocity and the pressure profile can be presented by a post-processing software, Paraview. What shown in Figure 5.10 is the velocity profile of one period at 120dB. Notice that the velocity around the edge is much higher than the other place. At the beginning of this period, the flow flows in the neck of the resonator and small vortices are triggered inside the neck. However, with the constraint of the wall of the narrow neck, the vortices disappeared very quickly. At the end of this period, when the flow flows out, much larger vortices are generated. Contrary to the narrow neck, the outflow does not have the restraint of the wall. So it is fully developed to a much larger scale. Also, notice that not only the flow inside the neck participates in the oscillation, there is still a small part of the flow outside the resonator which also participates in the oscillation. This is the reason why a length correction is needed in Section 4.1

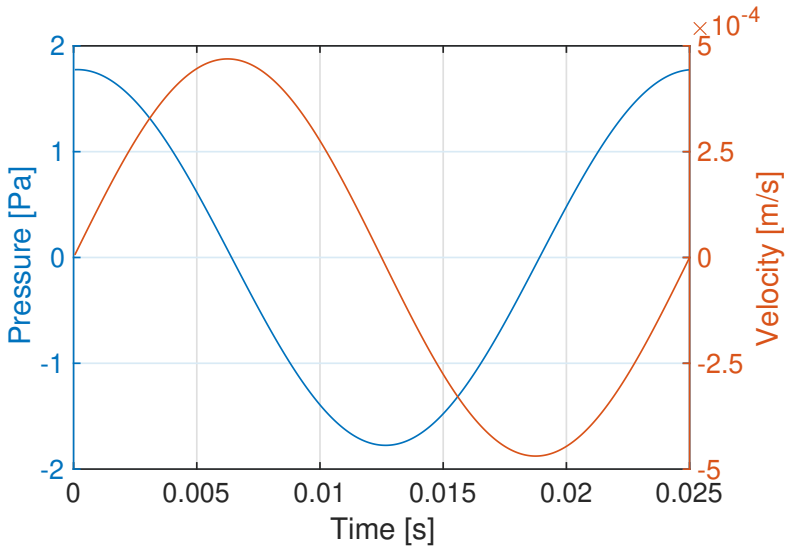

Figure 5.9: Velocity and pressure profile at the reference plane

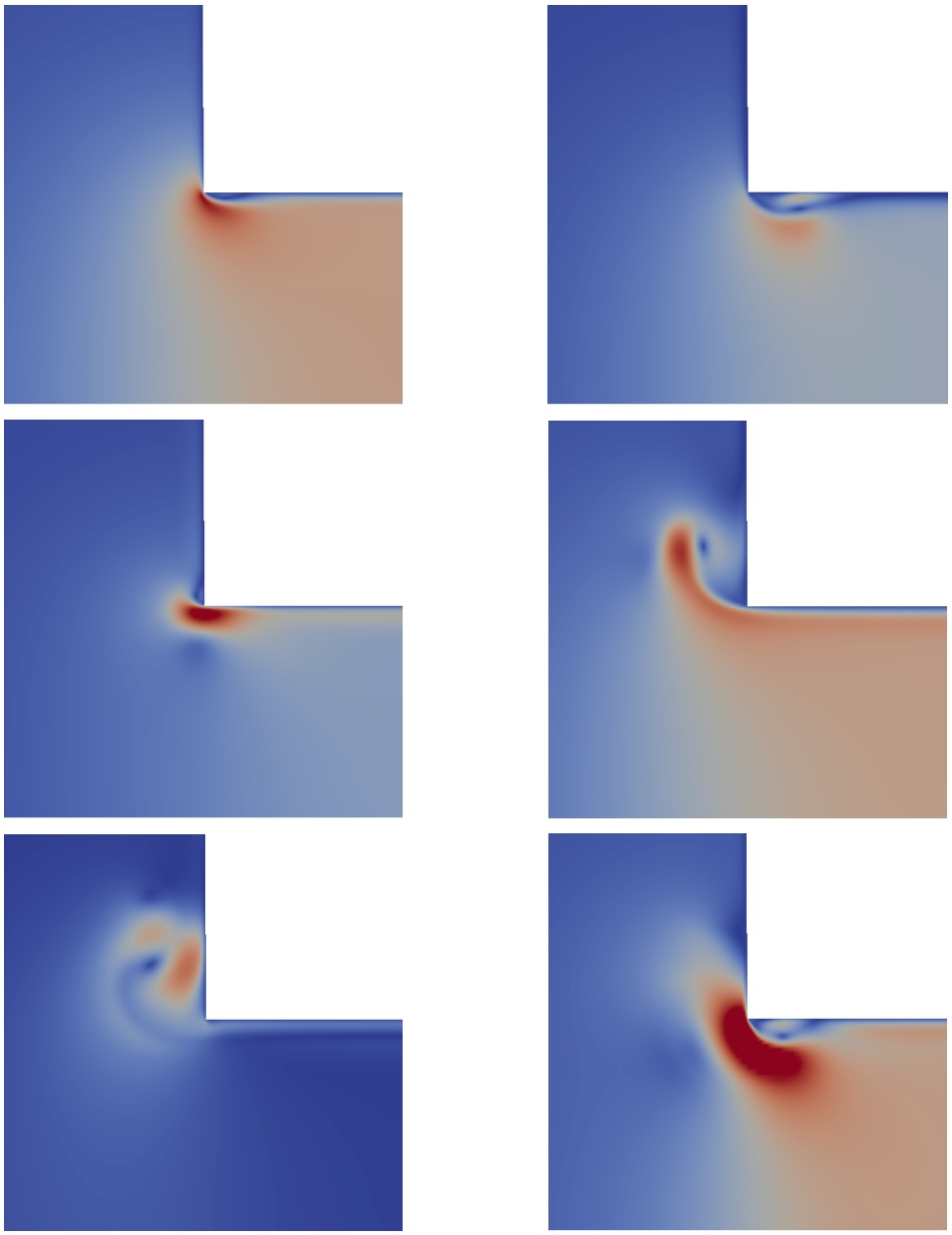

Figure 5.10: Vortices generated around the inlet of the resonator at 130dB

5.4.2 Damping Behavior at Different SPL

As mentioned in the previous chapter, the eigenfrequency of the Quarter wave resonator in this thesis is set as 400Hz and this numerical investigation is mainly focused on the damping behavior at the eigenfrequency at different SPL. Firstly, the normalized resistance of the Quarter wave resonator at different SPL is presented in Figure 5.11. At the lower SPL from 70dB to 90dB, the normalized resistance can be considered as constant. There are only very small changes taken place in these lower SPL. The normalized resistance starts to increase gradually at the higher SPL from 90dB to 130dB. At first, the increasing rate of the normalized resistance is rather small, but the higher the SPL is, the higher the increasing rate becomes. Notice that the normalized resistance exceed 1 at 130dB, which means that the damping manner changes from normal-damped to over-damped at 130dB. As for the gain of the reflection coefficient, as shown in Figure 5.12, it decreases very slightly at the lower SPL from 70dB to 90dB. The decreasing rate begins to rise from 90dB, as a result, the gain of the reflection coefficient decrease more significantly at the higher SPL. Notice that, the decreasing trend has not changed with the SPL range from 70dB to 130dB, even though the normalized resistance exceeds 1. However, it is also predictable that the gain of the reflection will start to increase at the SPL over 130dB. These results are similar to the analytical results and the comparison of both results will be further discussed in the next chapter.

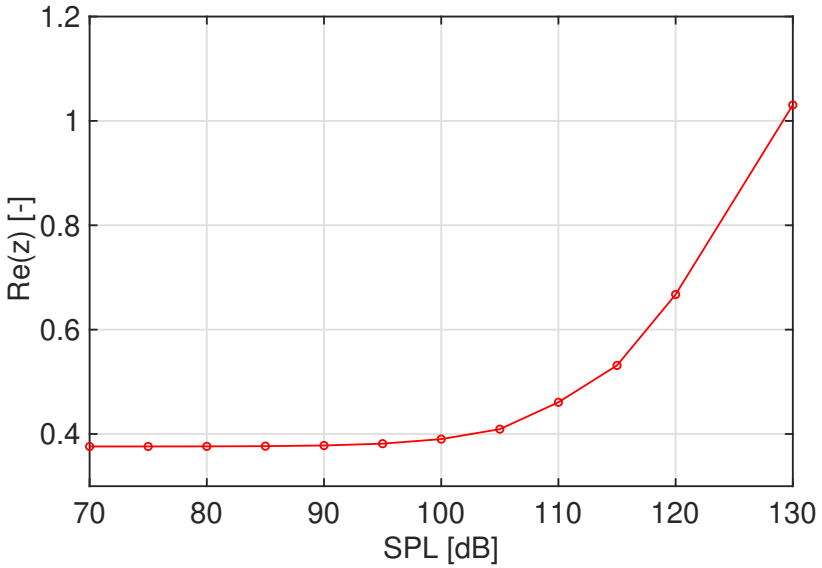

Figure 5.11: Normalized resistance of Quarter wave resonator at different SPL

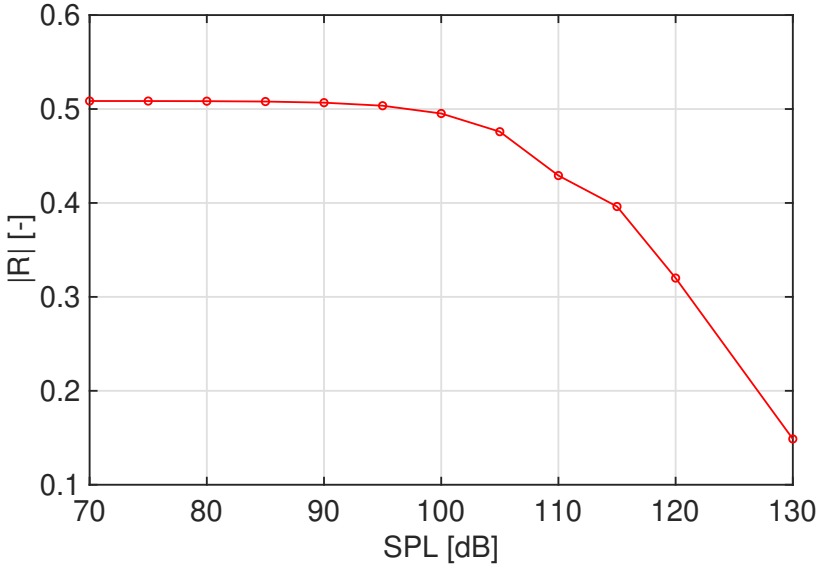

Figure 5.12: Gain of reflection coefficient of Quarter wave resonator at different SPL

6 Comparison of the Analytical Results and The Numerical Results

In this part of the thesis, the results from both analytical investigation(MATLAB) and numerical investigation(OpenFOAM) are compared with each other.

As shown in Figure 6.1, the starting point of the normalized of the analytical investigation is at around 0.3, but the starting point of the normalized of the numerical investigation is at around 0.4. Since at the lower SPL 70dB, the resistance is mainly caused by the friction, this difference indicates that the friction captured in the numerical investigation is larger than that in the analytical one. Furthermore, the normalized resistance in the analytical investigation shows a more obvious increasing trend than that in numerical one, since it starts to increase from 70db in the analytical investigation while it remains constant until 90dB. What's more, the normalized resistance in analytical investigation exceeds 1 at 120dB while in the numerical investigation, it exceeds 1 at almost 130dB.

Beside the normalized resistance, the gain of the reflection coefficient of both investigations is also compared, see Figure 6.2. The gain of the reflection coefficient of the analytical model is almost 0.6 while that of the numerical model is only 0.5, which means that the damping effect captured numerically is better than that captured analytically. Since the decrease of the gain of the reflection coefficient in the analytical model is more significant than that in the numerical model, the gain of the reflection coefficient in the analytical model becomes lower than that in the numerical model; And it reaches its minimum value at 120dB, which is a bit lower than that in numerical model. This indicates that the resonator in MATLAB transforms from normal-damped to over-damped a bit earlier than that in OpenFOAM. However, the overall trend is shown in the both Figure 6.1 and Figure 6.2 is similar and the damping behavior corresponds in some degree, which validates with each other.

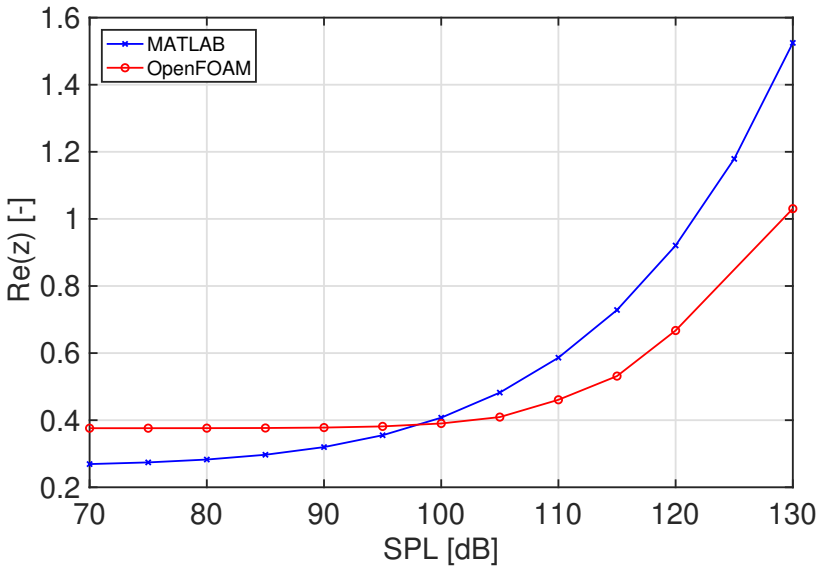

Figure 6.1: Normalized resistance at different SPL in analytical and numerical investigation

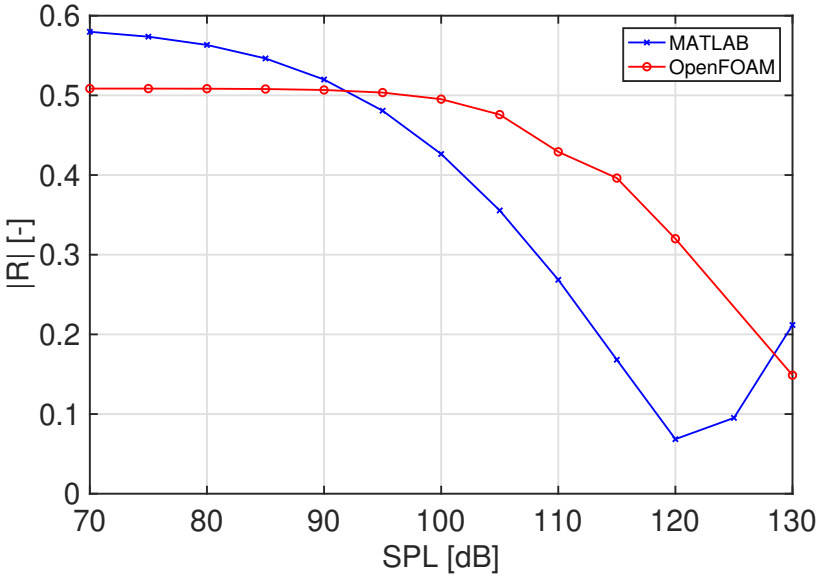

Figure 6.2: Gain of the reflection coefficient at different SPL in analytical and numerical investigation

6.1 Correction Based on the Comparison of Results

According to the comparison in the last section, the normalized resistance of the analytical and numerical investigation has a small deviation at the lower SPL range from 70dB to 90dB. Since at the lower SPL, the damping behavior remains in linear regime and the damping effect is mainly caused by the friction, which is a linear component. In this case, it is possible to implement a correction coefficient to the term which is responsible to the friction. According to Eq(4.2), the term $R_l u'$ take care of the thermo-viscous losses and it is a linear term. And this R_l is appropriate real-valued constant which might not accurately capture the frictions in the neck. Thus a correction coefficient η is added as follow:

$$R_{l,cor} = \eta R_l. \tag{6.1}$$

where the $R_{l,cor}$ denotes the corrected value. The correction coefficient is chosen properly so that the normalized resistance of both analytical and numerical investigation at the low SPL can be in good agreement. As shown in Figure 6.3, the corrected normalized resistance of the analytical investigation at 70dB is now the same as the results of the numerical investigation. After the correction, the normalized resistance of both investigations shows good agreement at the lower SPL. However, the deviation of the normalized resistance between the two investigations rises with the increasing SPL. The reason for this is that even though the linear damping effect has been corrected, there is still deviation in the nonlinear effect, i.e. the flow separation, which is not corrected. Since it is nonlinear, a correction coefficient is not sufficient. Thus, in this work, no further correction will be utilized.

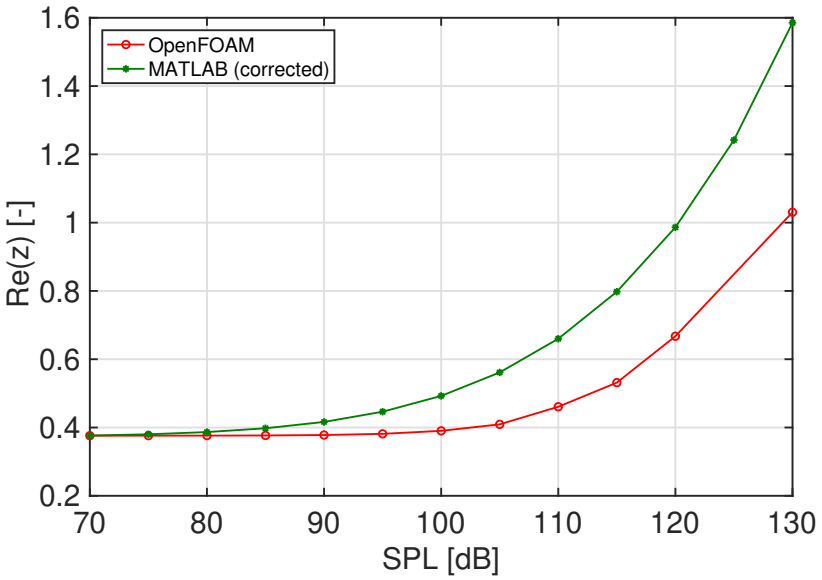

Figure 6.3: Normalized resistance at different SPL in analytical(corrected) and numerical investigation

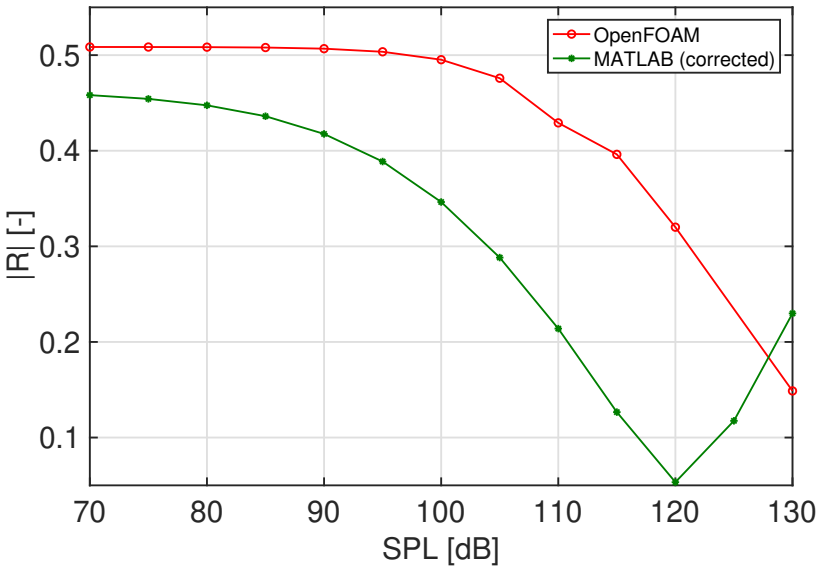

Figure 6.4: Gain of the reflection coefficient at different SPL in analytical(corrected) and numerical investigation

7 Summary and Conclusion

This work investigates the damping behavior of a Quarter wave resonator using an incompressible approach. The incompressible approach means that the flow in the should be considered as incompressible. To achieve this, the length of the neck should be small enough compared to the wavelength of the acoustic wave so that the neck can be considered as acoustically compact. When the neck is acoustically compact, the flow inside the neck can be treated as incompressible. Moreover, decomposition methodology, which was suggested by Ingard and Ising [7], is applied in this work. This methodology was well applied to the Helmholtz resonator and also to the Quater wave resonator done by Foerner [4]. And in this work, it is also implemented on the Quarter wave resonator. The investigation of the Quarter wave resonator in this work contains two part: the analytical part and the numerical part. The analytical investigation is implemented in MATLAB and the numerical investigation is utilized in OpenFOAM. Notice that the evaluation process of the numerical investigation is done in the MATLAB. The parameters of the Quarter wave resonator in both parts are set as the same in order to make sure the results are comparable. The focusing point of this work is the damping behavior at eigenfrequency and this is compared to the end of the work. Since there is a deviation between the two investigations, a reasonable correction is implemented.

Firstly, the goal was to set up the analytical model in the MATLAB. Based on the methodology mentioned above, the Quarter wave resonator was also decomposed into two parts: the neck and backing cavity; And they were investigated separately. Since the reflection coefficient, which an essential value to characterize a resonator, is a function of both frequency and SPL, there are two loops applied in this part of the investigation. In the first loop, the resonator was investigated only over the frequency spectrum. Initially, the pressure drop between to both ends of the neck was derived at every frequency. Then the pressure drop and the velocity were transformed from time domain to frequency domain using the MATLAB function: FFT. Then the impedance of the neck was computed by dividing the transformed pressure drop to the transformed velocity. The impedance of the backing cavity was calculated separately. Afterward, the total impedance was derived by adding the impedance of the neck and the backing cavity together and the reflection coefficient was also calculated. One very important key to this work is that the SPL at the reference plane should maintain constant as a target SPL. Due to the damping effect, the actual SPL at the reference plane was lower than the target SPL, iterations are implemented in the second loop to adjust the excitation amplitude of the incident acoustic wave, i.e. the amplitude of the velocity. The higher the SPL was, the more iterations needed. When the reflection coefficient of the resonator converged to an approaching value, which indicates the SPL at the reference plane was finally constant, this value was taken as the final result. Since there is no obvious dividing line between the neck and the

backing cavity, effects of different proportions of the neck were investigated. The changes of the proportion led to the shift of the eigenfrequency of the resonator and also the damping efficiency. As for the effect on the impedance, the proportions of the neck had more influence on the resistance than the reactance. What's more, at the lower SPL, the resistance remained at the linear regime. At the higher SPL, the resistance stayed at the nonlinear regime and the resistance at the eigenfrequency increased significantly. Notice that the change of the proportion did not have an effect on the reactance. Besides, the normalized resistance at the eigenfrequency raised with the increasing SPL and it exceeded 1 at around 120dB, which means the damping behavior transformed for normal-damped to the over-damped. Thus, the gain of the reflection coefficient decreased to the minimum and started to increase at 120dB.

Secondly, the similar methodology was implemented in OpenFOAM. In this work, only the neck was investigated in the OpenFOAM and the backing cavity still used the analytical model, since the incompressible assumption was only applied in the neck. In order to simplify the numerical simulation, only a wedge of the resonator was simulated. In order to achieve this, the wedge boundary condition was utilized. One difficulty in this part of the work was the mesh generation. The resolution of the mesh should be fine enough to capture the friction and the vortices. Several resolutions were simulated and the results showed only a slight deviation, which indicated the resolutions were all fine enough. Then the distance between the reference plane the should be chosen. According to [13], the position of the reference should not have an effect on the results. This was validated also in these simulations. There was only a slight deviation between the results of the simulations with different reference distance. There were two approaches mentioned in [13] to obtain the impedance of the neck. The simulation results at 70dB of both approaches showed good agreement. Then the simulation results of the neck are added together with the analytical results of the backing cavity and the same iteration process was utilized to main the constant SPL at the reference position. It only took one time of the iteration at the lower SPL while it took much more iterations at the higher SPL. Finally, at the eigenfrequency, the damping efficiency at different SPL was investigated. The normalized resistance increased with the increasing SPL and it exceeded 1 at around 130dB. Thus the gain of the reflection coefficient maintained a decreasing trend. However, it is also predictable that the gain of the reflection coefficient will also increase after 130dB since the resonator at 130 is over-damped.

Furthermore, the results of the analytical and numerical investigation were compared. In general, the trend of the curves of the normalized resistance and the gain of the reflection of the were similar but there were still deviations. In the analytical investigation, the resonator transformed from normal-damped to over-damped at 120dB while in the numerical simulation it transformed at 130dB. The deviation of the analytical and numerical investigation was rather small at the lower SPL but it increased with the increasing SPL. Since the linear regime is dominant at the lower SPL and the nonlinear regime is dominant at the higher SPL, the linear part of the both analytical and numerical showed rather good agreement but the nonlinear part was not. Therefore, a correction coefficient was applied to the linear term, i.e. the friction, to correct the deviation at the lower SPL. After the correction, the resistance at the lower SPL showed very good agreement while the deviation still increased with the increasing SPL. This indicates that the nonlinear part of the analytical and numerical investigation had deviation.

However, at this point, it is not possible to determine whether is the analytical investigation over-predict or the other way around. This can be determined when corresponding experiments are implemented.

Appendices

A MATLAB Script

A.1 Analytical Investigation

```
clear;
clc;
%% MATLAB SCRIPT OF ANALYTICAL INVESTIGATION OF QUATER-WAVE RESONATOR
%**************************************************************************
%% TARGET
SPL = 120;
% dB targert SPL at reference plane
f_eig_target = 400;
% 1/s eigenfrequency of the resonator
%% OVERALL PARAMETERS
l_ref = 0.00;
%reference length [m]
Pr_norm = 0.72;
%Prandtl number [-]
kappa_norm = 1.4;
%Ratio of specific heats [-]
M_norm = 0.0289644;
 %Molar mass [kg/mol]
T_norm = 293.15;
%Temperature [K]
R_norm = 8.3144598;
%Gas constant [J/kgK]
p_norm = 100000;
%Atmospheric pressure [Pa]
pa_norm = 20e-6;
%Commonly used reference sound pressure in air [Pa]
Rho_norm = p_norm * M_norm / (R_norm * T_norm);
%Density [kg/m^3]
c_norm = sqrt(kappa_norm * p_norm / Rho_norm);
%Speed of sound [m/s]
visk_dyn_norm = 17.1e-6;
%Dynamic viscosity [Pa s]
visk_kin_norm = visk_dyn_norm/Rho_norm;
%Kinetic viscosity [m^2/s]
%% GEOMETRICAL PARAMETER
d_0 = 0.00635;
%Diameter of the duct [m]
l_correction = 4/(3 * pi) * d_0;
```

```
%Length correction [m]
l_all = 1/4 * c_norm / f_eig_target;
%Total length of the QW Resonator [m]
l_0 = 0.02;
%Length of the neck of the QW Resonator [m]
l_e = l_0 + l_correction;
%Effective length [m]
l_cav = l_all - l_0;
%Length of the backing cavity [m]
Cd = 0.76;
%Vena contracta [-]
sigma = 0.0156;
%Porosity [-]
%% LOOP
j_limit = 100;
%Limit of the outer loop
frequency_range = 800;
%Range of the frequency spectrum
%% SET UP VECTORS
fft_Z = zeros(j_limit,frequency_range);
%Impedance [N s/m^3]
fft_R = zeros(j_limit,frequency_range);
%Reflection coefficient [-]
fft_Z_0 = zeros(j_limit,frequency_range);
%Impedance of the neck [N s/m^3]
fft_Z_bc = zeros(j_limit,frequency_range);
%Impedance of the backing cavity [N s/m^3]
amplitude_fft_R = zeros(j_limit,frequency_range);
%Gain of the reflection coefficient [-]
phase_fft_R = zeros(j_limit,frequency_range);
%Phase of the reflection coefficient [degree]
f_vec = linspace(25,(frequency_range + 24),frequency_range);
%frequency range 25-1000 Hz
A_u = zeros(j_limit,frequency_range);
%Amplitude of velocity [m/s]
R_eigen_freq = zeros(1,j_limit);

%% LOOP
flag_inertia = 1;
flag_viscosity = 1;
flag_flowseparation = 1;
flag_areajump = 1;
flag_backcavity = 1;
for j = 1:j_limit
%outer loop

    for k = 1:frequency_range
    % inner loop
        f = f_vec(k);
        %% PREPARETION FOR FFT FUNCTION
        N = 2000;
```

```
90          % Length of signal
91          fs = 2000 * f;
92          % Sampling frequency
93          t = (0:N-1)/(fs);
94          % Time vector
95          freq = (0:N/2) * fs/N;
96          %% VELOCITY
97          if j == 1
98               A_u(j,:) = 0.02;
99               %Initial guess of amplitude of velocity
100         end
101         u_vec = A_u(j,k) * sin(2 * pi * f * t);
102         %Velocity [m/s]
103         u_dt_vec = A_u(j,k) * 2 * pi * f * cos(2 * pi * f * t);
104         %Derivative of velocity
105         %% CALCULATE REAL-TIME VALUE R_l
106         s = 1/d_0 * (1 + (kappa_norm-1)/sqrt(Pr_norm)) * sqrt(2 * ...
               visk_kin_norm / (2 * pi * f));
107         %Boundary layer parameter [-]
108         R_l = s * Rho_norm * (2 * pi * f) * (l_e);
109         %Real-valued constant
110         %% CALCULATE PRESSURE
111         ∆_p_vec = flag_inertia * (Rho_norm * l_e / sigma * u_dt_vec)...
112                     + flag_viscosity * (R_l * u_vec/sigma)...
113                     + flag_flowseparation * (1/2 * Rho_norm * u_vec ...
                           .* abs(u_vec)/(Cd * sigma)^2) ...
114                     + flag_areajump * 1/2 * (Rho_norm * u_vec .* ...
                           u_vec * (1/sigma^2-1));
115                     %Pressure drop
116         %% FFT
117         fft_∆_p = fft(∆_p_vec,N);
118         fft_u = fft(u_vec,N);
119         %% CALCULATE THE IMPIEDENCE OF THE DUCT
120         fft_Z_0(j,k) = fft_∆_p(2)/fft_u(2);
121         %% CALCULATE THE IMPIEDENCE OF THE BACK CAVITY
122         fft_Z_bc(j,k) = flag_backcavity * (-1i * cot(2 * pi * f * ...
               l_cav/c_norm) * Rho_norm * c_norm/sigma);
123         %% CALCULATE THE IMPIEDENCE OF QW RESONATOR
124         fft_Z(j,k) = fft_Z_0(j,k)+ fft_Z_bc(j,k);
125         %% REFLECTION COEFFICIENT
126         fft_R(j,k) = (fft_Z(j,k) - Rho_norm * c_norm)/(fft_Z(j,k) + ...
               Rho_norm * c_norm);
127         %% CALCULATE THE AMPLITUDE OF VELOCITY FOR THE NEXT LOOP
128         A_u(j+1,k) =abs(1 - fft_R(j,k)) * 10^(SPL/20) * ...
               sqrt(2)*pa_norm/(abs(1+fft_R(j,k)*exp(-1i * 2 * pi * f * ...
               l_ref/c_norm))*Rho_norm*c_norm);
129         %% AMPLITUDE OF REFLECTION COEFFICIENT
130         amplitude_fft_R(j,k) = abs(fft_R(j,k));
131         %% PHASE OF REFLECTION COEFFICIENT
132         phase_fft_R(j,k) = angle(fft_R(j,k));
133     end
```

```
134      %% ACCURACY OF REFLECTION COEFFICIENT
135      if j ≥ 2
136        if ...
             abs((min(amplitude_fft_R(j,:))-min(amplitude_fft_R(j-1,:))))<1e-5
137        %0.00001
138        break;
139        %terminate the loop if the R approach a static value
140        end
141      end
142  end
```

A.2 Evaluation in Numerical Investigation

The MATLAB script of the two different approaches to compute the impedance of the neck.

```
1  % Calculate the derivative of velocity
2  diff_u(j,:)=diff(u(j,:))./diff(t);
3  %% FFT
4  fft_p = fft(p(j,:));
5  fft_u = fft(u(j,:));
6  fft_diff_u = fft(diff_u(j,:));
7  %% APPROACH 1
8  fft_Z_tot(j,1) = fft_p(2)/fft_u(2);
9  fft_Z_duct_pot(j,1) = 1i * Rho_norm * 2 * pi * f * (l_AB - l_0) * ...
       fft_u(2);
10 %Calculate the impedance
11 fft_Z_bc(j,1) = -1i * cot(2 * pi * f * l_cav/c_norm) * Rho_norm * ...
       c_norm/sigma;
12 fft_Z_0(j,1) = fft_Z_tot(j,1) - fft_Z_duct_pot(j,1);
13 %Substract the impedance from reference plane to the inlet of the ...
       resonator
14 fft_Z(j,1) = fft_Z_0(j,1) + fft_Z_bc(j,1);
15 fft_R(j,1) = (fft_Z(j,1) - Rho_norm * c_norm)/(fft_Z(j,1) + Rho_norm ...
       * c_norm)
16 %% APPROACH 2
17 ft_ᐞ_p = fft_p(2) - Rho_norm * (l_AB - l_0) * i * 2 * pi * f * fft_u(2);
18 fft_ᐞ_p = fft_p(2) - Rho_norm * (l_AB - l_0)  * fft_diff_u(2);
19 %Substract the pressure drop from reference plane to the inlet of the ...
       resonator
20 fft_Z_0(j,2) = fft_ᐞ_p/fft_u(2);
21 %Calculate the impedance
22 fft_Z(j,2) = fft_Z_0(j,2) + fft_Z_bc(j,1);
23 fft_R(j,2) = (fft_Z(j,2) - Rho_norm * c_norm)/(fft_Z(j,2) + Rho_norm ...
       * c_norm)
24 %Iterations in order to make sure the SPL at the reference plane is ...
       constant
25 A_u(j+1,1) =abs(1 - fft_R(j,1)) * 10^(SPL/20) * ...
       sqrt(2)*pa_norm/(abs(1+fft_R(j,1)*exp(-1i * 2 * pi * f * ...
```

```
      l_ref/c_norm))*Rho_norm*c_norm);
26 A_u(j+1,2) =abs(1 - fft_R(j,2)) * 10^(SPL/20) * ...
      sqrt(2)*pa_norm/(abs(1+fft_R(j,2)*exp(-1i * 2 * pi * f * ...
      l_ref/c_norm))*Rho_norm*c_norm);
```

Bibliography

[1] A. Cummings. Transient and multiple frequency sound transmission through perforated plates at high amplitude. *Journal of the Acoustical Society of America*, 79(4):942–951, April 1986.

[2] R. Piero E. Laudien, R. Pongratz and D. Preclick. Fundamental mechanisms of combustion instabilities: Experimental procedures aiding the design of acoustic cavities. *Liquid Rocket Engine Combustion Instability*, pages 377–399, Jan 1995.

[3] K. Förner and W. Polifke. Scattering to Higher Harmonics for Quarter-Wave and Helmholtz Resonators. *AIAA JOURNAL*, December 2016.

[4] Kilian H. Förner. Nonlinear aeroacoustic characterization of resonators. *journal acoustic*, March 2013.

[5] The OpenFOAM fundation. User guide. 2017.

[6] A. S. Hersh, B. E. Walker, and J. W. Celano. Helmholtz resonator impedance model, part 1: Nonlinear behavior. *AIAA Journal*, 41(5):795–808, May 2003.

[7] U. Ingard. On the theory and design of acoustic resonators,. *Journal of Acoustical Society of America*, 25(6):1037, November 1953.

[8] U. Ingard and H. Ising. Acoustic nonlinearity of an orifice. *The Journal of the Acoustical Sociaty of America*, 42(1):6–17, 1967.

[9] P. Martinez-Lera K. Förner, J. Tournadre and W. Polifke. Characterization of the nonlinear response of a helmholtz resonator. *Annual Report*, pages 33–45, 2015.

[10] W. Polifke I. Lopez Arteaga K. Förner, M. A. Temiz and A. Hirschberg. On the non-linear influence of the edge geometry on vortex shedding in helmholtz resonators. *22nd International Congress on Sound and Vibration (ICSV22)*, 2015.

[11] J.J. Keller and E Zauner. On the use of helmholtz resonators as sound attenuator. *Zeitschrift fuer angewandete Mathematik und Physik ZAMP*, 46(3):297–327, 1995.

[12] Ronald L. Panton and John M. Miller. Resonant frequencies of cylindrical helmholtz resonators. *Journal of the Acoustical Society of America*, 57(6):1533–1535, June 1975.

[13] Jonathan Tournadre, Kilian Förner, Paula Martinez-Lera, Wolfgang Polifke, and Wim Desmet. Determination of acoustic impedance for helmholtz resonators through incompressible unsteady flow simulations. *22nd AIAA/CEAS Aeroacoustics Conference*, May 2016.

[14] Qi Zhang and Daniel J. Bodony. Numerical investigation and modelling of acoustically excited flow through a circular orifice backed by a hexagonal cavity. *Journal of Fluid Mechanics*, 693:367–401, Jan 2012.